NTNU – Trondheim
Norwegian University of
Science and Technology

Uptake and biological response to zinc by the Diatom *Thalassiosira pseudonana*

Marit Eggen

Chemical Engineering and Biotechnology
Submission date: June 2012
Supervisor: Olav Vadstein, IBT
Co-supervisor: Matilde Chauton, IBT

Norwegian University of Science and Technology
Department of Biotechnology

Acknowledgments

The present study is a continuation of the specialization project conducted at the Department of Biotechnology autumn 2011. Both studies were written within the project SOLBIOPTA - Biotechnological Production of Materials for Optimized Solar Cell Efficiency, a collaboration project between SINTEF Materials and Chemistry and the NTNU departments Materials Science and Engineering, Biotechnology and Biology. SOLBIOPTA has a highly interdisciplinary character involving various scientific fields. This is also reflected in the present study in which sciences like algae-biology, element chemistry and physics, and nanotechnology are present and have mutual effects on each other. The complexity of this combination introduced many challenges during planning and developing adequate procedures that could contribute to reach the proposed aims of the project. Many of the original aims and objectives had to be reassessed when they proved to be over-ambitious or non-feasible, and new were formed during the course of the project. Due to the multitude of analytical techniques and methods utilized in this project, the theory and utilization of each technique has been limited to include a short, basic description within the section of Methods and Materials. For further information the reader is advised to look to the references cited therein.

I would like to thank post.doc. Matilde Chauton for irreplaceable guidance and help in the laboratory, and also for her valuable advice and evaluation of my work throughout the project. I would also like to thank Olav Vadstein for his advice and superb knowledge of the biology of phytoplankton, Dr. Lasse M. Olsen for his help in developing the objectives and the implementation of the project, Senior Engineer Syverin Lierhagen for providing me with ICP-MS results, John Walsmsley for the EDS analysis, and Julien Romann for providing me with excellent SEM pictures. Finally, a special thank to my friend and fellow student Sophie Glas for kindly proofreading my texts.

Sammendrag

I denne studien ble opptak- og inkorporeringspeksperimenter av sink gjennomført på en Si-, Co- og Zn-sultet *Thalassiosira pseudonana*-kultur. To eksperimenter ble gjennomført der en forhåndsbestemt mengde av en sinksulfat-løsning og en natriummetasilikatnonahydrat-løsning ble tilsatt en eksponentielt voksende semi-kontinuerlig algekultur for å få ønsket startkonsentrasjon i mediet. Eksperiment 1 og 2 hadde en startkonsentrasjon av sink på henholdsvis 8.3 µM (høydose) og 1.7 µM (lavdose). Hvert eksperiment ble gjennomført i batch-modus med en varighet på 48 timer. Hyppig prøvetaking i første del av eksperimentet ble gjennomført for å følge biologisk opptak av de tilsatte metallene. Den biologiske reponsen til sinktilsetningen i algekulturen ble fulgt under forsøket ved måling av fotofysiologiske parametere (F_t og Q_Y), organisk karbon- og nitrogeninnhold, celletall, optisk tetthet, samt næringskonsentrasjoner (PO_4^{3-} og NO_2^-). Endringen i konsentrasjonen av sink og silikat i medium og organisk materiale ble fulgt ved ICP-MS analyse. Struktur og elementkomposisjon av kiselalgefrustulene ble videre analysert gjennom bruk av Scanning Electron Microscopy og Energy Dispersive X-ray Spectroscopy. Endringen i den cellulære fraksjonen av sink fulgte en celleoverflate-metall sorpsjonsprosess i to faser, hvorav fase én innbefattet høy initiell adsorpsjon av metall på celleoverflaten etterfulgt av en gradvis desorpsjon av metall fra celleoverflaten i fase to. Høy økning av pH i mediet etterfulgt av utfelling av sink som sinkhydroksider antaes å være hovedårsaken til den observerte sorpsjonstrenden, da partikulært sink har festet seg til celleoverflaten. Andre mulige årsaker er kompleksering av sink gjennom interaksjon med metabolske produkter utfelt fra aktivt fotosyntetiserende og voksende celler. Redusert biologisk tilgjengelighet av sink kan ha ført til redusert opptak av metallet i algene. Sammenlignet med frustuler fra ubehandlede kiselalger var det allikevel en høyere fraksjon av sink i frustulene fra de eksperimentelle kiselalgekulturene. Det høyeste innholdet av sink ble detektert i frustulene fra lavdoseeksperimentet og tilsvarte en mengde sink relativt til silikat ($\mu gZn\ \mu gSi^{-1}$) på 5.16% for 24 h-prøven og 0.146% for 48 h-prøven. På grunn av den store forskjellen i sinkfraksjonene mellom frustuleprøvene fra dette eksperimentet kombinert med mulig kontaminering fra vaskeprosedyren (H_2O_2) brukt på frustulene fra dette forsøket er det relatert høy usikkerhet til disse fraksjonene. Allikevel kan en høyere fraksjon i lavdose eksperimentet forklares med høyere biologisk tilgjengelighet av sink på grunn av lavere totalkonsentrasjon og påfølgende lavere andel partikulært sink i dette eksperimentet. Ingen klar biologisk respons kunne direkte knyttes opp mot sinktilsettingen, og den observerte reduksjonen i fotofysiologisk tilstand mot slutten av eksperimentene ble relatert til silikat-sulting.

Abstract

The uptake and incorporation of zink by a Si-, Co- , and Zn starved *Thalassiosira pseudonana* culture was examined. Two experiments were conducted in which a predetermined amount of a zinc sulfate solution and sodium metasilicate nonahydrate solution were delivered to an exponentially grown fed-batch algae culture yielding the wanted start concentrations in the medium. Experiment 1 and 2 had final zinc concentration of 8.3 µM (high dose) and 1.7 µM (low dose), respectively. The experiments were conducted in batch mode for 48 hours. Frequent sampling during the first part of the experiments were performed in order to examine the biological uptake of zinc and silicate. The biological response to zinc addition was followed throughout the experiment by measuring photo-physiological parameters (F_t og Q_Y), organic carbon and nitrogen content, cell density, optical density, and nutrient concentrations (PO_4^{3-} and NO_2^-). The concentration development of silicate and zinc was followed in the uptake assay samples through ICP-MS analysis. The structural and elemental composition of the diatom frustules were later examined through the use of Scanning Electron Microscopy and Energy Dispersive X-ray Spectroscopy, respectively. The cellular zinc development followed a two-phase sorption process in which first phase consisted of rapid metal binding to cellular surfaces followed by a gradual desorption of zinc from the cells in the second phase. High initial pH-increase followed by precipitation of zinc as hydroxides is assumed to be the main reason explaining the observed sorption trend, explicitly through the attachment of particulate zinc to cellular surfaces. Other possible explanations are assigned to complexation of zinc by organic exudates excreted from actively photosynthesizing and growing cells. Reduced biological availability of zinc may have led to decreased metal uptake by the algae. However, a higher fraction of zinc was present in the experimental frustules as compared with frustules from untreated algae culture. The highest amount of zinc was detected in the low-dose experiment corresponding to a weight-fraction relative to silicate of 5.16% for the 24 h-sample and 0.146% for the 48 h-sample. Due to the high inter-sample difference in zinc fraction combined with possible sample-contamination from chemicals or equipment through the cleaning process (H_2O_2) used on the frustule samples from this experiment, these fractions are connected with high uncertainty. No explicit biological response to zinc addition was observed in the algae cultures in either of the two experiments, and the reduction of the photo-physiological condition observed by the end of the experiments were related to silicate-depletion of the culture medium.

List of abbreviations

CA	Carbonic Anhydrase
CM	Control experiment with medium
dSi	Dissolved silicate
DSSC	Dye Sensitized Solar Cell
dZn	Dissolved zinc
EDS	Energy Dispersive Spectroscopy
EDTA	Ethylenediaminetetraacetic acid
Exp1.HD	Experiment 1 High Dose
Exp2.LD	Experiment 2 Low Dose
f/2	Sea water medium designed for growing diatoms
FSD	Fractional Standard Deviation
ICP-MS	Inductively Coupled Plasma Mass Spectrometry
MtIII	Class III metallothioneins
OD	Optical Density
PSII	Photosystem II
RSD	Relative Standard Deviation
SDS	Sodium Dodecyl Sulfate
SDV	Silicon Deposition Vesicle
SIT	Silicon Transport
S(T)EM	Scanning (Transmission) Electron Microscopy
UC	Ultra Clave

List of symbols

$\mathbf{BE}$	Biomolecules containing exchangable ions
$\mathbf{BL}$	Biomass binding sites
$\mathbf{BM}$	Biomolecules containing metal ions
$\mathbf{D}$	Dilution rate
$\mathbf{D_c}$	Critical dilution rate
$\mathbf{E_M}$	Metal uptake rate
$\mathbf{F_t}$	Instantaneous chlorophyll fluorescence
$\mathbf{K_M}$	Metal binding affinity constant
$\mathbf{k_{in}}$	Rate constant of metal transport across membrane
$\mathbf{M}$	Metal ions
$\mathbf{M_{bio}}$	Biological metal
$\mathbf{M_h}$	Hydrophilic metal
$\mathbf{M_{int}}$	Internalized metal
$\mathbf{M_L}$	Lipohilic metal
M-SH	Metal bound to thiol groups
$\mathbf{N_T}$	Cell number at time T
$\mathbf{N_0}$	Initial cell number
$\mathbf{T}$	Transport molecules
$\mathbf{V_{inn}}$	Flow of medium into the culture
$\mathbf{V_{max}}$	Maximum rate
$\mathbf{V_{total}}$	Total culture volume
$\mathbf{Q_Y}$	Quantum yield
$\mathbf{X}$	Biomass
$\boldsymbol{\mu}$	Growth rate
$\boldsymbol{\mu_{max}}$	Maximal growth rate

Contents

1 Introduction

1.1 The potential of diatoms

During the last decades our planet has experienced a major industrialization and technical advancement introducing smarter solutions and easier living to humans around the globe. At the same time these developments, together with increased human activity, require continuous access to energy. While the petroleum resources was, and still is, a pre-requisite for the realization and continuation of industrialization and technical development the side-effects of its use and exploitation can no longer be ignored. One of the major challenges facing us today is therefore to find and develop efficient ways to make use of renewable energy sources that do not impose further pressure on the environment.

In the search for inspiration and solutions our focus has turned to nature itself, which through millions of years has shaped and developed various living organisms displaying abilities that still are beyond any human-made advancement. The widespread unicellular algae, called diatoms, with their numerous species and morphological characteristics, are but one of many organisms that in recent years have received much attention for biotechnological applications. Due to the lipid and amino-acid rich content of diatoms these microalgae have for some time been used in the production of food in aquaculture [42, 7], biodiesel [46, 67], and more recently as providers of amino and fatty acids to pharmaceutical production [38, 40]. With the advent of (bio) nanotechnology, focus has been centered upon their highly elaborate cell wall, the frustule, consisting of biosilicate and surrounding each cell as a petri dish. Due to the various mechanical and optical properties of the frustules, these structures show a promising potential in applications ranging from drug-delivery vesicles, semiconducting devices, and as integrated metal-biosilicate composites in solar cells for enhanced solar capturing efficiency. In this context, information on how diatoms assimilate different trace metals, may provide knowledge of how one by altering medium composition and growth conditions can yield tailored diatom frustules with wanted properties. To reach this point, knowledge of the specific biology and cellular response of diatoms under various external metal conditions will be important.

1.2 The nature and life of diatoms

Diatoms are unicellular, photosynthesizing algae, also called phytoplankton, that belong to the group of *Phaeophyceae* (brown algae) [65]. They are found throughout the world's oceans and freshwater systems mainly in the surface photic layer where they receive sufficient light to support growth and primary production. Diatoms are estimated to be responsible for approximately 20% of global carbon fixation and represent around 40% of the 45 to 50 billion metric tons of organic carbon produced each year in the sea [77]. Apart from the importance of these organisms as major contributors to the overall carbon-life cycle, they also represent a primary food source to other aquatic organisms.

1.2.1 Diatom structure and function

The different shapes and sizes of diatoms are numerous. They can vary from circular to triangular with sizes between five to a few hundred micrometers. These organisms share typical characteristics with the standard plant cell: they have a nucleus containing

DNA, mitochondria, chloroplasts for photosynthesis, and a cell membrane [77]. Each cell contains one or more chloroplasts, often brown in color, although the color may vary with taxon and can even be greenish in some species [66]. However, the by far most distinguishing feature of the diatom structure is the elaborate and self-assembled micro and nanoporous outer cell wall, the frustule [55]. This highly elaborate structure is composed of two parts, or valves; called the epitheca and the hypotheca. Each valve is associated with a series of bands called girdle bands or cingulum that holds the two valves together. The cingulum are in most diatoms perforated strips of silicate, but in other species they can also be folded to form channel-like structures [66]. The epitheca is slightly larger than the hypotheca and encloses the former as a lid on a petri dish. Through cell division the epitheca of each new diatom is the valve inherited from the mother diatom while the hypotheca is synthesized during the cell division [66].

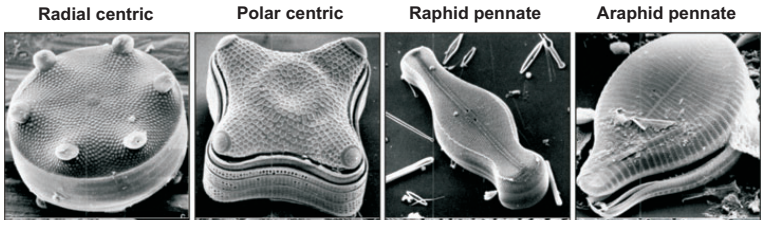

Figure 1.1: Scanning electron microscopy of four different diatom species representing centric and pennate symmetry [36]

The pore pattern on the frustule-valves is highly species-specific and makes the basis for diatom categorization. According to the pore-symmetry on the frustule, diatoms are thus divided into two main groups, namely the centric diatoms, having a radial symmetry, and pennate diatoms, having a symmetry along a bilateral line. These main groups can further be divided into two sub-groups, the raphid and araphid pennate diatoms, and the radial and polar centric diatoms [36]. Different diatoms representing centric or pennate symmetry can be seen in Figure 1.1. In some species, like in the centric diatom *Coscinodiscus sp.,* the frustule valves consists of three overlapping porous layers in which the pores may have a decreasing or increasing pore diameter going from the outside to the inside (Figure 1.2).

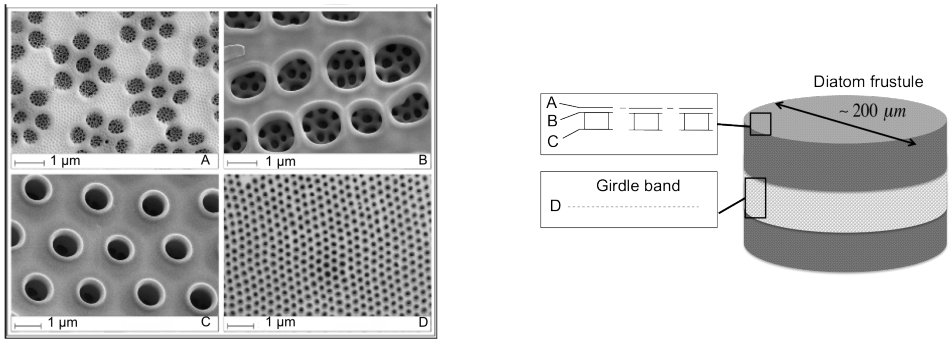

Figure 1.2: A schematic presentation of a centric diatom frustule with cross-sectional profile of the silicate wall. The three layers, A, B, and C are indicated in the right figure with corresponding SEM images of the layers from a *Coscinodiscus sp.* frustule in the left figure. Picture: Julien Romann, NTNU.

In these species the upper pore layer, the cribellum, has the finest pores. The middle plate, the cribrum, separates the two other layers and contains pores of intermediate diameter. The inner pores sitting against the cribrum surface are the largest and are referred to as the foramen [43]. Another and historically important diatom is *Thalassiosira pseudonana.* This centric diatom can vary in size from 2-15 μm in diameter, and is known as a model diatom belonging to a genus widely distributed around the globe, and whose genome was the first of the eucaryotic phytoplankton to be sequenced (see Virginia Armbrust *et al.* (2004) [77]). This algae may occur as single cells or in chains of up to 6 cells. Its frustule is characterized by having a ring of protruding processes around the edges of the valve-face and costae. An additional feature often found in the diatom-frustules from the *Thalassiosira*-order is the central tubular process called the central fultoportulae. These structures penetrate the silicate framework and is thought to function as an excretion channel for β-chitin fibrils [66, 63]. The function of the chitin is not yet fully understood, but recent studies suggests that the chitin may function as a scaffold structure for silicate deposition [9]. The pores on the frustule surface are spherical and irregularly arranged with a narrow size distribution ((18.3±3.1) nm in diameter) [59]. Figure 1.3 shows SEM pictures taken of a *T.pseudonana* washed with SDS/EDTA. The fibre-like structures that can be seen in the left picture are thought to be chitin. The right picture reveal some of the specific frustule details.

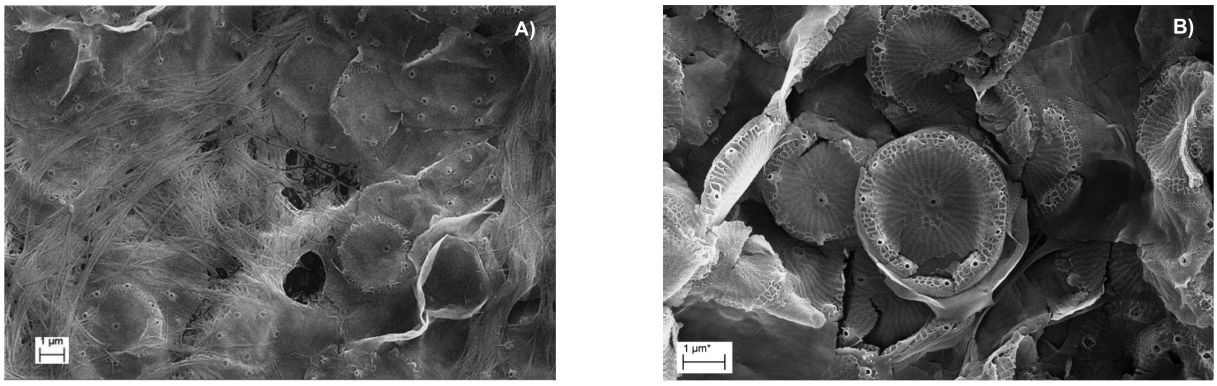

Figure 1.3: SEM pictures of SDS/EDTA washed *T.pseudonana* culture

Diatom frustules are covered with a 3D-network of organic material mainly composed of polysaccharides and proteins. This layer is connected to a variety of surface moieties like amino, carboxyl and silanol groups that control both surface charge, and affinity to metal ions [21, 20].

Frustule function The intricate nanostructured pattern of the frustule has been linked to a wide variety of functions, such as light guides for increased light harvesting efficiency in photosynthesis, and as mechanical protection against turgor pressure and predators. The high symmetry of the pore structure in the different layers and the pore-size distribution encountered in some species provide the frustule with unique optical properties. Yamanaka *et al.* (2008) investigated the optical properties of the frustule from the fresh water diatom *Melosira variance.* They showed that light absorption was mainly in the blue light-region. They also deduced that the cribrum and areola layers beneath the cribellum may function as light distribution devices efficiently irradiating chlorophylls inside the cell [90]. These findings may provide a good explanation for the high light-

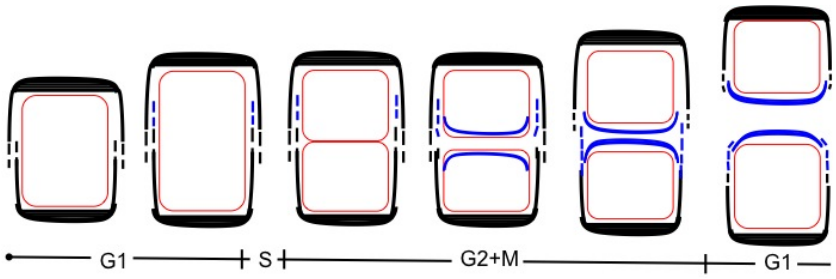

Figure 1.4: Diagram of cell cycle events in *Thalassiosira pseudonana*. The different stages (G1, S, and G2+M) are denoted at the bottom. The upper and lower lines represents valves, dashed lines on sides represent girdle bands. Valves and girdle bands of the mother cells are black, and those of the newly synthesized are blue. The red box within the valves and girdle bands represents the cytoplasm. Adapted from Hildebrand *et al.* (2007) [30].

harvesting efficiency displayed by many diatoms along with the fact that chloroplasts has been shown to be located in close proximity to the cell wall [43, 19]. Another important function of the frustule is to provide mechanical protection against harsh physical conditions and predators. C. E. Hamm *et al.* (2003) performed various stress tests on three diatom species differing in both size and symmetry. Their results showed that the frustule possessed remarkable strength that was inversely correlated with the frustule size [27].

1.2.2 Life cycle and reproduction

As for most other unicellular organisms the diatoms reproduce vegetatively by binary fission [29]. The cytokinesis and production of new valves both occur while being surrounded by the intact cell wall of the mother cell. This leads to the production of two new cells where one of the cells have the same size as the parent cell, while the other, which inherit the parent hypotheca as its epitheca, will have a reduced size. This form of reproduction leads to a decrease in cell size after each mitotic division (see Figure 1.4). When the cell size has reached 30-40% of its original value, the diatom responds with sexual reproduction [66]. The sexual reproduction starts with meiotic cell division producing gametes (haploid cells). Two gametes fuse together to form a zygote (the fertilized egg) (see Figure 1.5). The diatom life cycle is therefore characterized by the alternation between a vegetative phase and a rejuvenation phase followed by sexual reproduction. The sexual reproduction ensures the restoration of the original cell size through the formation of an auxospore. Having but a thin membrane, the auxospore is flexible and allows for an expansion of the cell while it is growing. The frustule production starts within the auxospore when the cell has reached the maximal size [29].

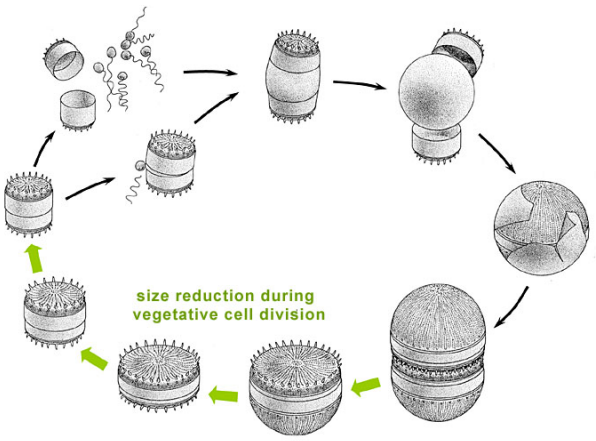

Figure 1.5: A schematic representation of the reproduction cycle of a centric diatom. Also included is the sexual reproduction [63].

1.2.3 Silicon biomineralization and formation of the frustule

Much attention has been given to the understanding of the mechanisms controlling the uptake and biomineralization of silicate by diatoms and the molecules involved in this process. Even though recent studies have contributed tremendously to the understanding of the mechanisms involved (see [35, 66, 64, 39, 75, 45]) there are still aspects with the process of biosilicification and morphological development of the frustule that are not yet fully understood.

Diatoms are the world's largest contributors to silicate-biosilicification, which makes silicate the major limiting nutrient for diatom growth [45]. The concentration of oceanic silicate today is approximately 70 μM, but local silicate concentrations in natural waters vary significantly [8]. The diatom frustule is composed of hydrated amorphous silicate (biosilica) with the general formula $[Si_nO_{2n-(nx/2)}(OH)_{nx}]$, $x \leq 4$. The overall process of silicification involves transport of the silicate across the plasmalemma and through the cytoplasm to the so-called silicon deposition vesicle (SDV), in which the silicate polymerization occurs [45]. Chisholm *et al.* (1978) proposed the existence of intracellular silicate pools in which the silicate would be stored prior to being polymerized and incorporated through the SDV [13]. The existence and size of these pools depend strongly on the diatom specie but also on environmental variables such as light intensity and micronutrient concentrations [69]. The diatom cell takes up silicate through an aerobic process by the aid of specific proteins called silicon transport proteins (SIT proteins) [8]. The preferred form of silicate for uptake is orthosilicic acid ($Si(OH)_4$), which comprises about 97 % of the dissolved Si (dSi) in seawater at pH 8.0. The remaining Si in seawater under these conditions exists primarily as $SiO(OH)_3^-$ [45]. A unique property of silicic acid, compared to other nutrients is that it autopolymerizes into silicate polymers (fibers) at concentrations above 2 mM at neutral pH. Despite this, intracellular Si-pools in diatoms have shown to contain concentrations well above the saturation level, varying from 19-340 mM [75]. The processes controlling the uptake of silicate from the surrounding medium are influenced by several factors including expression and localization of transport proteins, and the rate of silicate biomineralization and incorporation into the cell wall. Three modes of silicic acid uptake have been suggested; surge uptake, internally controlled uptake, and exter-

nally controlled uptake. The surge uptake is characteristic for silicate-starved cells with deplete silicate pools and its uptake kinetics represent the maximal uptake rate of silicic acid. The internally controlled uptake represents the case in which the uptake control is exerted by the rate of intracellular utilization of the silicate, presumably the rate of silicate incorporation into the cell wall. Limiting extracellular silicic acid concentrations control the uptake kinetics in the externally controlled uptake [45].

1.3 Metal-cell interactions

1.3.1 Metal toxicity and interaction with cellular surfaces

Diatoms are known to have a high affinity towards a variety of dissolved trace elements and they will therefore exert a strong control on the transfer of heavy metals along the water column to the sediments. Along with the fact that they constitute one of the fundaments in the trophic food chains they are also responsible for much of the bioaccumulation of certain heavy metals, in particular Cd and Zn, throughout the web of food chains [20]. The study of the toxicity and bioaccumulation of metals in diatoms will therefore help understanding to which degree these metals will proceed to other organisms, and also how the diatoms control the metal concentration in freshwater and marine environments. Figure 1.6 shows the various metal binding sites and processes involved in the biosorption of metal to algal cells.

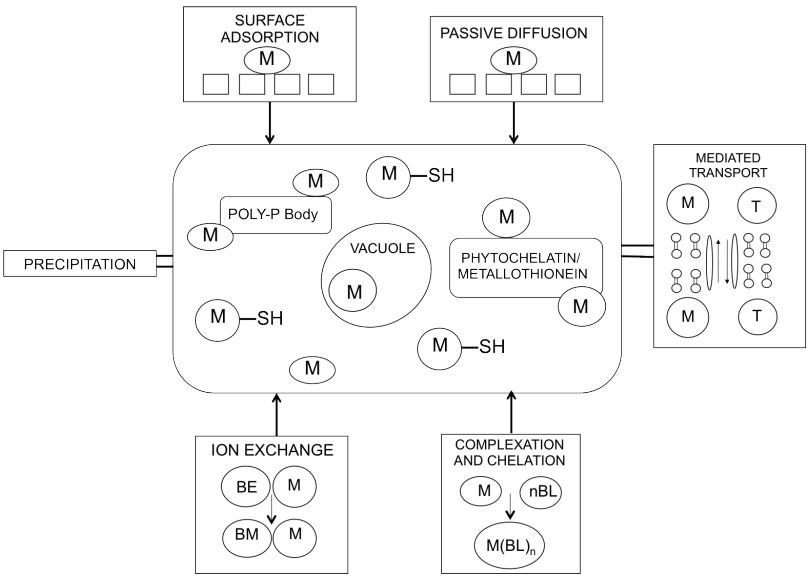

Figure 1.6: Schematic representation of processes involved in microalgal biosorption of metals. M, metal ions; T, transport molecules; BE, biomolecules containing exchangeable ions; BM, biomolecules containing metal ions; BL, biomass binding sites; M-SH, metal bound to thiol groups. Adapted from Monteiro *et al.* (2012) [50].

Toxicity The toxicity of metals towards diatoms depends on several factors, some of which are pH and metal speciation. Metal-organism interactions and toxicity are generally believed to be controlled by the concentration of the free metal ions and not the total metal concentration [22, 47]. As a result of the major differences in metal tolerance between species, phytoplanktons have developed various ways of controlling the uptake and

reducing the toxicity of metals at high concentrations. The following defense mechanisms have been observed: (i) The development of energy-driven efflux systems to keep the intracellular concentration of toxic elements under the critical level, (ii) enzymatic conversion of the oxidation state of the metal to a less toxic form, (iii) precipitation of metal complexes on the cell surface, (iv) complexation of metals with excreted metabolites, (v) conversion of toxic metals into volatile species, (vi) intracellular complexation with proteins or polysaccharides, and (vii) intracellular enzymatic methylation of the metal that may prevent it to react with thiol groups (–SH) [22, 50]. Also metal exclusion in the sense of having less metal-reactive surface is a proposed defense mechanism [17]. The factors controlling complexation of metals by metabolic products or waste excreted from cells have been much studied and are thought to be normal mechanisms to both enhance and restrict the bioavailability of metal ions [22]. Fisher *et al.* (1984) observed different complexation patterns displayed by log-phase and senescent cells concerning which metals that were preferentially bound. This phenomenon was connected with the different compounds excreted by the cells in the two physical states. The authors also proposed that certain algae species could obtain higher capacity to accommodate cellular metal concentrations through precipitation of metals as sulfides [17]. Along with the physical state of the cells the production of extracellular compounds also depends on environmental factors such as temperature, salinity, nutrient concentrations, light intensity, and on the presence of toxic compounds in the medium. As mentioned, another prominent defense mechanism in order to decrease internal metal concentration adapted by certain plants and eukaryotic algae, is the production of specific intracellular peptides or proteins capable of binding metals. These molecules, as organometallic-complexes, are further partitioned inside vacuoles providing the microorganisms with the possibility of neutralizing potentially toxic concentrations of certain metals. In literature these peptides are divided into two groups; (1) the enzymatically synthesized short-chain polypeptides, named phytochelatins (or class III metallothioneins, MtIII) found in higher plants, algae, and certain fungi, and (2) the gene-encoded proteins: class II metallothioneins (identified in cyanobacteria, algae and higher plants) and class I metallothioneins found in most vertebrates. It has been shown that synthesis of MtIII can be enhanced by the presence of heavy metals such as Pb^{2+}, Zn^{2+} and Cu^{2+} [80].

Metal-cell surface interaction The toxicity and uptake of metals by phytoplankton cells are processes that are highly dependent on the specific interaction chemistry between the metals in question and the elemental composition and thickness of the cell surface. Gélabert *et al.* (2006, 2004) demonstrated that the main contribution of metal adsorption came from the organic layer covering the frustules as compared to the frustule itself. This layer contains a variety of functional groups including carboxyl ($-COO^-$) and silanol ($-SiO^-$) groups that can bind metal ions and, which under normal sea or freshwater pH-values, provide the cellular surface with an overall negative charge [21, 20]. Various studies on cell surface-metal interactions suggest that carboxyl groups contribute to the major part of proton and metal binding sites [58, 21], and various attempts have been made to develop models for the binding of metals based on this surface-metal-complex formation [89, 21]. Uptake of metals will normally proceed according to a process which involve the following steps (see Figure 1.7): (i) Diffusion of the metal from bulk solution to the biological surface; (ii) Sorption/surface-complexation of the metal at passive binding sites within the protective layer or at sites on the outer surface of the plasma membrane; and (iii)

Uptake or 'internalization' of the metal [11].

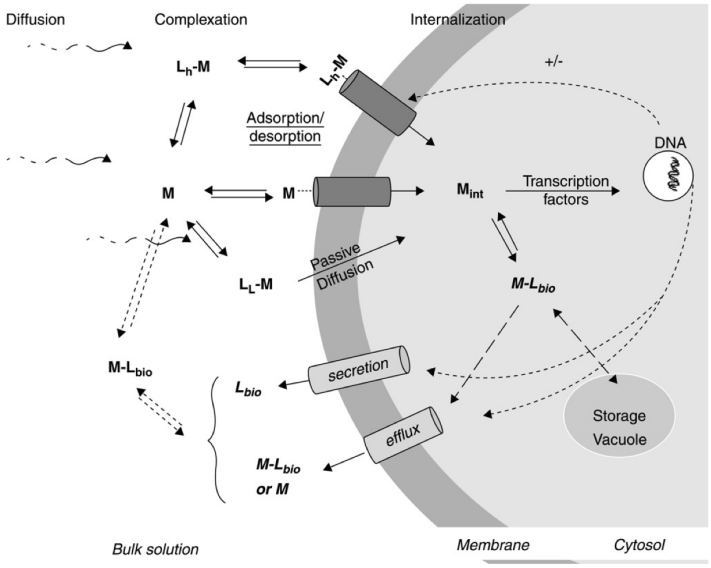

Figure 1.7: A descriptive representation of some of the important processes leading to and following uptake of trace metals by aquatic microorganism. L, ligand that can complex metal; M_L, lipohilic metal, M_h, hydrophilic metal; M_{bio}, biological metal; M_{int}, internalized metal [86].

1.3.2 Zn bioactivity, availability and incorporation

Zn solubility and concentration in seawater The concentration of dissolved Zn (dZn) in seawater varies greatly with depth and between oceanic- and coastal waters. The concentration of dZn in oceanic waters has been found to be 10^{-10} M. In coastal waters the concentration has been found to be 100-1000 times the oceanic value [71], and much of this large difference is assigned to metal contaminations in effluents from industrial facilities, agriculture, or other human activities.

Bioactivity of Zn Zn is an essential nutrient for most diatoms as it makes part of various metalloenzymes in the cells. It has for instance been shown that Zn acts as a cofactor in the enzyme carbonic anhydrase (CA), which converts inorganic bicarbonate (HCO_3^-) into CO_2 for photosynthesis [83], as well as in alkaline phosphatase and 5' nucleotidase, which are enzymes involved in the extracellular cleavage of phosphorous from organic compounds. Zn also plays a role in the metabolism of DNA as it makes part of DNA and RNA polymerases. Another proposed function for Zn is related to the Si-metabolism were it activates a conserved motif in the Si-transporter proteins [79]. At high concentrations Zn may affect and inhibit the oxidizing side of photosystem II (PSII) by non-competitively inhibiting Ca^{2+} and Mn^{2+} by binding to their native sites on water oxidase resulting in reduced photosynthetic performance [48]. This inhibition of the electron transport is partially due to the change in the ultrastructure of the thylakoid membrane as well as the destruction of antennae pigments [49, 61]. Zn also stands in an antagonistic relationship with manganese, another important nutrient for diatoms [74]. The Zn requirement varies between diatom species but also between coastal and oceanic diatoms within the same species. For instance it has been shown that the coastal phy-

toplankton tend to have higher Zn requirements than their open-ocean counterparts [14]. This requirement is an effect of the already mentioned difference in ambient trace metal concentration between the coastal and oceanic waters. At low external Zn concentrations the utilization of cobalt (Co) or cadmium (Cd) as a replacement for Zn has been shown to be a mechanism utilized by some diatoms [60, 51, 72, 92]. Through their study of Zn limited growth on the marine diatom *Thalassiosira weissflogii,* Morel *et al.* (1994) indicated that Co and Cd could restore the carbonic anhydrase activity [51]. Later it was confirmed that Co could alleviate Zn limitation by in vivo substitution in the enzymatic complex of CA [92].

Uptake and bioavailability of Zn The uptake kinetics of Zn are believed to follow the mechanisms developed for other trace metals (as postulated in 1.3.1). In literature it is normal to divide the uptake of Zn in two phases; phase one consisting of rapid sorption of Zn to surface ligands, and the much slower second phase in which the sorbed metal is being subject to active uptake or intracellular uptake by passive diffusion. The rate at which the metals are taken up strongly depends on their chemical state. Zn in its free divalent ionic form (Zn^{2+}) is the preferred state for uptake by diatoms, and the ability to predict this concentration is therefore important in studies where this type of control is needed. At steady state conditions, the amount of metal bound to the transporter, and therefore the metal uptake-rate, can be described by the saturation equation:

$$E_M = \frac{V_{max}[M]K_M}{[M]K_M + 1} \tag{1.1}$$

where [M] is the concentration of the free metal ion or kinetically labile inorganic species (the free ion plus dissolved inorganic complexes), and K_M is the affinity constant for the binding of metal M to the transport site. V_{max} (equation (1.2)) is the maximum rate achieved at metal saturation of the transport sites, and is equal to the total number of moles of transporter per unit biomass (X) times the rate constant (k_{in}) for the transport of metal across the membrane and subsequent release into the cytoplasm.

$$V_{max} = k_{in}X \tag{1.2}$$

Cells may utilize more than one transport system in the uptake of various nutrient metals. These transport systems differ in their affinity towards the metal in question, and depending on the chemical conditions such as low versus high metal ion concentration, different transport systems will dominate the metal uptake. Kinetic studies of Zn uptake by various eukaryotic algae, among them diatoms, have given indication of the existence of at least two transport systems for this metal: (1) a high-affinity system (log K_{Zn}= 9,6-10,0) controlled through a negative feedback system; and (2) a low-affinity system that is either constitutive or under minimal regulation [73]. The study of the uptake and incorporation of Zn by the diatom *T. pseudonana*, performed by Ellwood *et al.* (2000), indicated that under low Zn concentrations the uptake kinetics were under diffusional limitation, while under Zn-replete conditions the diatom controlled the uptake rate such that it remained more or less constant over time [14].

The bioavailability of Zn to marine organisms has been extensively studied, and different models have been constructed to calculate metal speciation and complexation of Zn under different conditions. These studies include the speciation of metal ions under different pH

conditions [93, 10] and complexation with chelator species such as EDTA [70]. Based on available thermodynamic stability constants and individual ion activity coefficients Alberto Zirino *et al.* (1972) constructed a pH-dependent model for the speciation of various metal ions in seawater. The distribution of chemical Zn species in seawater as a function of pH was calculated at 25 °C and 1 atmospheric pressure (see figure 1.8).

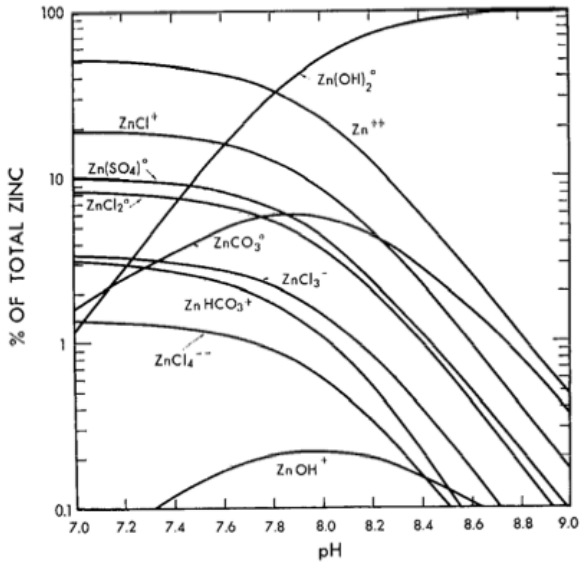

Figure 1.8: Calculated distribution of the chemical species of Zn in seawater at 25 °C and 1 atm as a function of pH [93]

The concentration of intracellular metal in phytoplankton is influenced by the day-night cycle. Carbon fixation, which only can occur during the light period, affects the growth rate of the cells, and since metal uptake may take place during both day and night a significant biodilution of the intracellular metal concentration may occur at the end of the light period [73]. Low levels of oceanic Zn has forced phytoplankton to adapt by decreasing their cellular Zn requirement. The mechanism by which this is done is not clear, but one possibility is the replacement of Zn in enzymatic sites by other chemically similar metals such as Cd and Co, as previously mentioned [14].

Frustule incorporation Even though culturing studies have shown that the majority (>97%) of Zn in diatoms is present in the organic material, trace amounts of Zn have also been found as integrated parts of the frustule, with the amount deposited following a positive correlation with the free ion concentration of Zn in the surrounding medium [2, 14]. The mechanisms behind Zn incorporation in the frustule is not yet fully understood. However, in literature two models are most common: a passive and an active mechanism. The first model implies that Zn is passively incorporated into the frustule, with the amount deposited reflecting the amount of Zn present within the diatom's internal cellular pool. The second model implies that Zn may play a role in the formation of the frustule [14]. Jaccard *et al.* (2009) studied the uptake and incorporation of Zn into the frustule of the freshwater diatom *Stephanodiscus hantzschii*. They reported a sigmoidal relationship between the molar Zn/Si ratio of the frustule composition. They also found a strong correlation between the intracellular Zn concentration and the Zn associated with the

diatom frustule. They further illustrated that manganese and Zn may compete for frustule incorporation [32]. In the study performed by Ellwood *et al.* (2000) the amount of incorporated Zn in the frustule of the diatom *T. pseudonana* represented 1-3% of the total amount of Zn taken up by the diatom [14].

1.4 Theory and advantage of the continuous culture

The study of microbial cultures and the physiological effects caused by different variables such as limiting nutrients, toxic pollutants, or external factors such as pH or temperature, is highly dependent on systems in which control of growth rate and nutritional addition may easily be achieved. Also for the procession of the various 'omics '-technologies, such as metabolomics and genomics, in which cell physiology on a molecular level is characterized, careful control of the cultivation process and the possibility of reproducible conditions are of high and often inevitable importance. The advent of the continuous culture system, the chemostat, by Monod (1950) and Novick and Szilard (1950) facilitated the conduction of studies of this nature [31].

Cultures of different microbial systems can in general be divided in two main groups; batch and continuous. In a batch culture there is no material input or output. Because of the simplicity of its design, this type of system was historically the most used. Here the population growth increases until a specific level is reached, at which a key nutrition becomes the limiting factor. Since there is no exchange of material during population growth, any produced material will accumulate, and the batch culture will therefore be a highly dynamic system with continuously varying substrate concentration, microbial population and physiology of the organisms. In the continuous culture there is a constant exchange of nutrient and biomass, keeping the system in a constant condition and thus controlling the population growth [62]. This represents the major advantage in the continuous culture; the possibility to grow the microbial population at a constant rate and controlling or varying environmental factors such as pH, nutrient concentration and metabolic products. In this system there is a balance between the influx of new medium and the efflux of spent medium and excess cells. There are different types of continuous cultures, for examle the chemostat and the turbidostat. In the chemostat fresh growth medium, in which a key nutrient is limited, is introduced to the system at a constant rate. The growth of new biomass will therefore be equal to the rate of which the culture is being diluted by new medium.
The rate of medium fed to the culture is based on the volume in the culture vessel, and is defined by the dilution rate D,

$$D = \frac{V_{inn}}{V_{total}} \tag{1.3}$$

where V_{inn} is the flow of medium into the culture and V_{total} is the total culture volume. The change in biomass (X) over time under steady-state growth can be expressed as

$$\frac{dX}{dt} = \mu X - DX \tag{1.4}$$

Where μ, the specific growth rate, is defined as the increase in biomass per unit time. This equation may be rewritten as

$$\mu = D + \frac{dX}{dt} \cdot \frac{1}{X} \tag{1.5}$$

At steady state conditions, dX/dt=0 and the specific growth rate can be defined as

$$\mu = D \tag{1.6}$$

This enables the manipulation of the growth rate provided the dilution rate is kept below the critical dilution rate (D_c), the rate at which the steady-state biomass concentration is unchanged [62, 31].

1.5 Future applications of diatoms and diatom frustules

Diatoms represent an exciting source of potential applications spanning from pharmaceutical products and cosmetics utilizing intracellularly synthesized fatty acids and amino acids, respectively [38], to the production of photovoltaic cells as light harvesting devices. In fact the intricate frustule was formerly used to test the resolution of optical microscopes [77]. Today diatoms are cultivated in large quanta to be used as food for marine organisms such as shrimps [38], and a great interest in diatoms and frustules has become evident in the fields of material science and nanotechnology. Some of the proposed applications for diatoms and diatom frustules are outlined below.

Molecular separation For efficient molecular separation a symmetrical and hierarchical pore structure is desirable and often inevitable. The frustule of some diatoms has therefore been proposed to provide a template for 3D-engineered nanostructured materials. This approach has been used to produce meso to macroporous hierarchical carbon material [43]. Others have proposed to use diatom frustules in purification of water and in gel filtration [56].

Heavy metal removal in wastewater Traditional techniques used in the removal of heavy metals from wastewater include physical treatments like ion exchange, membrane filtration and adsorption, and chemical treatments like chemical precipitation, flotation and evaporation [53, 81]. Many of these methods suffer from low removal efficiency and high cost. In addition several methods pose a threat to the environment due to utilization of hazardous chemicals and energy-requiring equipment. Owing to their high biosorption ability and their natural high abundance in oceans and lakes the use of algae in removal of heavy metals from effluents and wastewater has arisen as an inexpensive and efficient alternative to chemical and physical treatments [47, 50].

Sensing Biosensors are devices that incorporate a biological molecular-recognition component connected to a transducer that creates a signal of which strength is proportional to the concentration of the material being sensed. A common problem within the field of biosensing is the accumulation of molecules around the sensors that may interfere with the signal. Controlling the accessibility of the sensor is an important step to avoid this problem, and may be achieved using diatom frustules as sensor-platforms [56].

Photonic crystals Photonic crystals are periodically structured materials which possess photonic bandgaps. These bandgaps are frequency ranges in which light propagation does not occur through the material [69]. The highly ordered pore structure and the limited thickness of the silicate wall are properties of the frustule that may enable their use as photonic crystals. Through the optical investigations on the frustule of the diatom *Coscinodiscus granii*, Fuhrmann *et al.* (2004) showed that the silicate cell wall functioned

as a photonic crystal-slab waveguide that can be used in various applications such as microresonators [19].

Dye sensitized solar cells (DSSC) Dye sensitized solar cells represent a technically and economically favorable alternative to the conventional photovoltaic devices. They also introduce material advances such as flexibility that enables them to be used in harsher and more exposed environments. The main difference between the conventional solar cell and the dye sensitized solar cells is that in the DSSC the light absorption and charge carrier transport is separated [24]. Figure 1.9 show a traditional DSSC (A) and a DSSC with incorporated monolayer of diatom frustules (B). When the dye is excited by a photon the electron is transferred to the conduction band [12]. Carriers are then transported in the conduction band of the semiconductor to the charge collector [24]. The electron donated from the dye to the conduction layer is replaced by an electron donated by the electrolyte that covers the dye and which again is connected to the cathode. Despite excellent reviews [23, 26] these types of cells suffer from low light-capturing efficiency. A novel attempt to increase the efficiency is to incorporate diatom frustules or metal-doped frustules in a monolayer onto the photo-anode. The structural characteristics of the frustules contribute to enhance the photo capturing efficiency by acting as integrated reflectors or even as photonic crystals, and the semiconducting nature of the metal-silicate composite facilitates the flow of electrons [68, 19, 33]. Different metals that may enhance the conduction capacity of diatom frustules has been proposed, amongst which are titanium, zinc and yttrium.

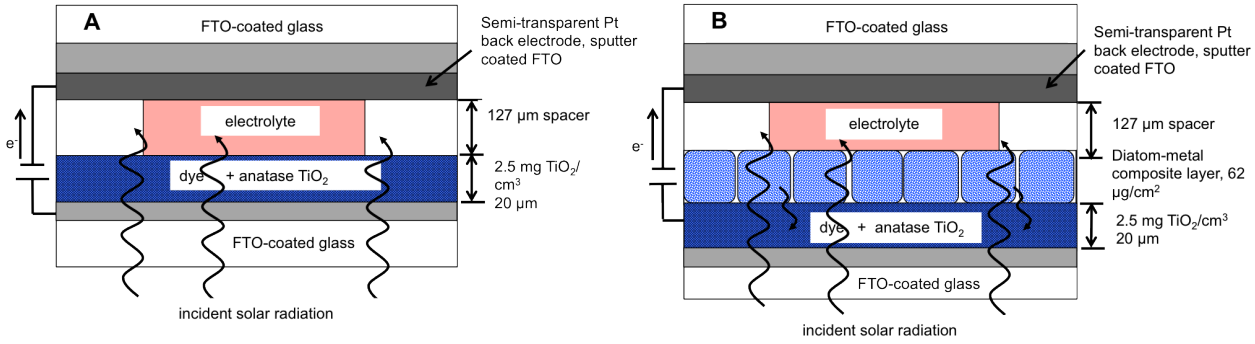

Figure 1.9: A: Traditional DSSC. B: DSSC with incorporated reflective diatom-metal composite layer. Adapted from Jeffreys *et al.* (2008) [33].

1.6 Aim of work

In this project we wanted to address the following issues; (i) the biological response to Zn addition on a Zn-, Co- and Si-deplete *Thalassiosira pseudonana* culture at two different metal concentrations, (ii) study the uptake of Zn, and (iii) if and to what degree incorporation of Zn into the biosilicate frustule of the diatom had taken place.

2 Materials and methods

2.1 Diatom used in the present study

The diatom *Thalassiosira pseudonana* was chosen for the investigation of the uptake kinetics and frustule incorporation of Zn.

2.2 Culture setup

2.2.1 Stem culture development

For the stem culture development the diatoms were inoculated in 800 mL non-adhesive polystyrene tissue culture flasks (BD-Falcon). The flask-cap was replaced by a silicate stopper, through which silicon tubes provided a means of leading air in and out of the cultures. Air was provided by a regular aquarium pump (Sonic 388) and was a means of keeping the cells in suspension as well as giving a source of carbon. The algae were grown in a closed climate chamber with a constant temperature of 20 °C equipped with fluorescent tubes providing 130 micromoles photons m^{-2} s^{-1} and 16:8 hours light-dark cycles.

2.2.2 Setup for exponential fed-batch cultivation

In the exponential fed-batch cultivation the cell cultures were held in the same type of culture flask as described in Section 2.2.1. Culture medium together with pressurized air was fed to the cultures through a silicon tube. A specialized pumping system supplied the medium at a set feeding-rate calculated as 2/3 of the maximum growth rate of the cells (μ_{max}). The experimental setup was placed in the climate chamber described in Section 2.2.1.

Figure 2.1: Setup for fed batch cultivation

2.3 Experimental design

Experimental preparation The photobioreactor was set up as depicted in section 2.5. All of the *T.pseudonana* utilized in this study originated from the same stem culture. To avoid differences, the two experimental cultures were kept in the same climate chamber and provided medium from the same container. The experimental medium had a final dSi concentration corresponding to approximately 50%, f/2 concentration, and only background levels of Zn and Co (0.11 µM and 8.48 x 10^{-4} µM, respectively) were present. In this way experimental diatoms in a Si-, Zn-, and Co-deplete condition could be obtained. Fluorescence parameters, optical density and dSi content were measured daily. Nitrate (NO_2^-) and phosphate (PO_4^{3-}) concentrations were also determined regularly to ensure that the cells did not suffer from nutrient deficiency. The experimental cultures were grown on the modified culture medium for several days in fed-batch mode until the optical density had stabilized and sufficient culture volume had been achieved. Both cultures were characterized by having high quantum yields.

Zn uptake studies In order to assess any concentration-dependent differences in the response and uptake pattern of *T.pseudonana* two different Zn concentrations were applied. Experiment one, designated as Exp1.HD (HD for 'High Dose'), and experiment two, designated as Exp2.LD (LD for 'Low Dose'), were conducted with a final Zn concentration of approximately 8.3 µM and 1.7 µM, respectively. These concentrations were chosen so as to expose the cells to Zn concentrations significantly different from the background levels of the medium. Based on the steady-state cell density and the pg Si per cell value calculated during the exponential phase of the preparation culture development, an appropriate amount of silicate solution was added to yield a concentration in the experimental medium enough to support one cell division. The PO_4^{3-} and NO_2^- concentrations were measured one day in advance to ensure that the cells were not affected by nutrient limitations at the onset of the uptake assays. The Zn stock solution had been stirred with a magnet stirrer for at least two hours prior to the experiment to avoid any presence of concentration gradients.

Each experiment was initiated by cutting off the medium supply and adding simultaneously via Eppendorf pipet the appropriate amount of Zn and Si stock solutions. After adding the solutions the culture flask was gently shaken to avoid cell and metal concentration gradients. At pre-determined time points samples of approximately 50 mL were withdrawn by the aid of a 60 mL syringe attached to a silicon tube leading into the culture. The sample was then distributed into three graduated cylinders for approximate volume measurements after which they were poured into the Millipore sampling manifold for filtration (described in Section 2.5). Figure 2.2 shows the various steps performed for each sampling. The accurate volume of the filtrates was measured after the filtration procedure by weighing the centrifuge tubes. Each experiment lasted for 48 h and the pre-determined sampling points were 0, 2, 4, 8, 16, 30, 60 min, and 24 and 48 h after the addition of Si and Zn. In addition a "pre-zero" sample, designated as the true zero in the following results, was taken from the preparation culture a few minutes before the experimental initiation to assess the current elemental concentration in the cultures. For Exp2.LD two additional sampling points, one at 3 h and one at 6 h after experimental initiation were included to obtain a higher resolution in the culture development. During

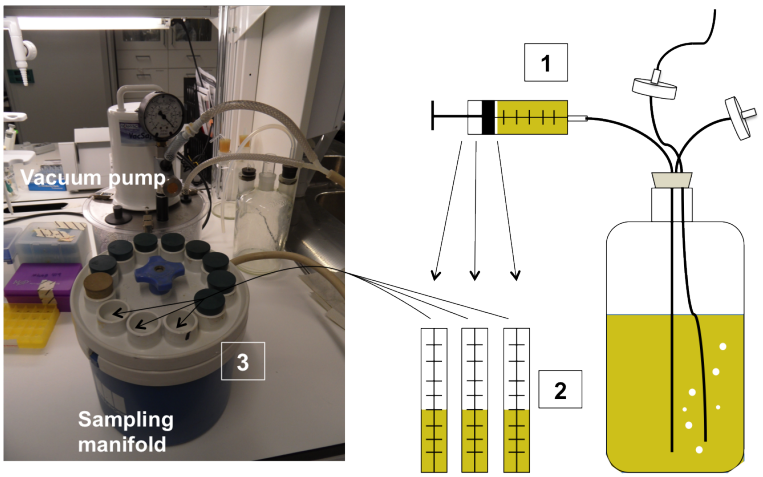

Figure 2.2: Descriptive set-up for the culture filtration. (1) 50 mL sample is withdrawn from the culture and (2) split into triplicate subsamples before (3) filtration.

the assays the various variables assessed included fluorescence variables, nutrient concentrations (dSi, PO_4^{3-} and NO_2^-), cell density, pH, optical density, and organic carbon and nitrogen content (C/N). Due to limited culture volume these variables were only assessed at some of the sampling points.

Control experiment and blank samples One control experiment, designated CM (Controll with cell-free culture medium), was performed in order to analyse the behavior of Zn when added to medium without cells and to see if any metal could get attached to the walls and bottom of the culture flask. The CM was performed with the same experimental procedures and equipment but with algae-free culture medium and Zn and silicate concentrations corresponding to the high dose experiment (8.38 µM Zn and 64.8 µM dSi). In order to see if any Zn contamination could arise during the filtration-step a triplicate "blank-sample" consisting of Milli-Q water was performed. In addition, analyses were done on filters that had been soaked in one of the triplicate tubes of filtrate from each sampling point in Exp2.LD and subsequently put on the sampling manifold to remove excess filtrate. This was done in order to quantify the fraction of detected metal in the filter samples that originated from the culture medium due to wet filters. The ratio between the elemental quantity in the soaked filters and the respective sample from which it was taken was calculated and the average of these ratios were used as correction factor in the filter analysis (see A table A.9 and table A.8). The control experiment and the blank samples were subsequently used to correct experimental samples. Table 2.1 shows the experimental parameters utilized.

Table 2.1: Experimental parameters for Exp1.HD, Exp2.LD and CM

Experiment	**Initial volume (mL)**	**Initial average cell number (mL^{-1})**	**Initial [Zn], M**	**Initial [dSi], M**	**Initial calculated pg Si $cell^{-1}$**
Exp1.HD	730	$8.7 \cdot 10^5$	$8.34 \cdot 10^{-6}$	$6.4 \cdot 10^{-5}$	1.5
Exp2.LD	715	$1.4 \cdot 10^6$	$1.67 \cdot 10^{-6}$	$6.4 \cdot 10^{-5}$	1.23
CM	810	-	$8.38 \cdot 10^{-6}$	$1.2 \cdot 10^{-4}$	-

Zn incorporation At the sampling points 24 h and 48 h aliquots of approximately 50 and 200 mL, respectively, of the remaining cell culture were harvested and cleaned for frustule component and structural analysis. The Exp1.HD frustules were cleaned with the SDS/EDTA method, but because of observed impurities in these samples it was chosen to utilize the H_2O_2 method for the Exp2.LD frustule samples. In addition frustules from an untreated algae culture grown on regular f/2 medium were analysed for elemental and structural comparison with experimental frustules. An aliquot from this culture was divided into two sub-samples: one was treated with the SDS/EDTA method, while the other was treated with the H_2O_2 method.

2.4 Medium preparation

2.4.1 Preparation of growth medium

The algae were grown in f/2-medium based on the recipe by Guillard (1975) [25] using seawater obtained from the Trondheimsfjord. Small particles and pollutants in the seawater were removed by filtration using a vacuum pump through a 90 mm glass microfiber filter with retention down to 1 µm. Filtered seawater was then sterilized by autoclaving at 120 °C for 60 minutes, and stored in a dark room at 4 °C until required. In order to prevent growth limitation caused by vitamin deficiency the added amount of vitamin stock solution was doubled in the medium preparation. f/2-medium was kept in 2 L microwave sterilized plastic flasks. A detailed description of the components present in the f/2-medium is presented in table 2.2.

Table 2.2: f/2 medium composition

Component	**Type of nutrient**	**Concentration in final medium (M)**
$NaNO_3$	Macronutrient	8.82×10^{-4}
$NaH_2PO_4 \cdot H_2O$	Macronutrient	3.62×10^{-5}
$Na_2SiO_3 \cdot 9H_2O$	Macronutrient	1.06×10^{-4}
$FeCl_3 \cdot 4H_2O$	Trace metal	1.17×10^{-5}
$Na_2EDTA \cdot 2H_2O$	Trace metal	1.17×10^{-5}
$MnCl_2 \cdot 4H_2O$	Trace metal	9.10×10^{-7}
$ZnSO_4 \cdot 7H_2O$	Trace metal	7.65×10^{-8}
$CoCl_2 \cdot 6H_2O$	Trace metal	4.20×10^{-8}
$CuSO_4 \cdot 5H_2O$	Trace metal	3.93×10^{-8}
$Na_2MoO_4 \cdot 2H_2O$	Trace metal	$2.60\text{x } 10^{-8}$
Thiamine · HCl (Vitamin B_1)	Vitamin	5.92×10^{-7}
Biotin (vitamin H)	Vitamin	4.1×10^{-9}
Cyanocobalamin (vitamin B_{12})	Vitamin	7.38×10^{-10}

2.4.2 Preparation of Zn solution

The Zn solution used in the experiments was based on $ZnSO_4$ dissolved in Milli-Q water and was kept in a stopped 100 mL volumetric flask. The exact Zn concentration ($4.56 \cdot 10^{-3}$ M) was determined by ICP-MS.

2.5 Analytical methods

Cell density The cell density (cells mL^{-1}) of the *T.pseudonana* cultures was quantified by visual counting in a Bürker chamber. Samples (2 mL) were collected and fixated with 50% glutaraldehyde (100 µL) and kept in the dark at 2 ^{o}C before they were counted. At the time of counting each sample was mixed thoroughly and counted in a specified area of the Bürker chamber for up to 12 times. The average of this value was then converted to cells per mL by using equation (2.1).

$$\frac{\text{cells}}{\text{mL}} = \frac{\text{counted cells}}{\text{number of squares}} \cdot \frac{1}{\text{volume of each square [mL]}} \tag{2.1}$$

The reported value for each sample point is the average of up to three countings.

Growth rate and doubling rate The maximal growth rate, μ_{max} (d^{-1}), and generation time (d^{-1}) of *T.pseudonana* was calculated from a batch culture were daily measurements followed the growth development. The natural logarithm of the optical density (OD) during the exponential growth phase were plotted against time. A linear regression of this plot provided the maximum growth rate as the slope of the curve. Dividing the maximum growth rate by ln(2) gave the generation time. The average cell specific growth rates, µ (d^{-1}), for the experimental cultures were calculated by using equation (2.2), where N_0 and N_T are the initial and final cell number, respectively, and T is the total experimental time period (in hours).

$$\mu = \frac{ln\left(\frac{N_T}{N_0}\right)}{T} \cdot 24\frac{\text{h}}{\text{day}} \tag{2.2}$$

Average Zn and Si uptake rates Average Zn and Si uptake rates were calculated from changes between the initial and final element concentration measured in the filter samples divided by the specific change in cell number of this time-period (equation 2.3).

$$\frac{\text{mol Zn (or Si)}}{\text{cell} \cdot \text{day}} = \frac{\frac{mol}{L}\,\text{Zn (or Si), filter, t=48h} - \frac{mol}{L}\,\text{Zn (or Si), filter, t=0}}{\left(\frac{cells}{L}\,\text{t=48h} - \frac{cells}{L}\,t{=}pre0\right) \cdot t_{\text{final (h)}}} \cdot 24\frac{\text{h}}{\text{day}} \tag{2.3}$$

pg Si per cell content The silicate content of *T.pseudonana* was calculated from the dSi and cell density development during the exponential growth phase of the algal culture (equation (2.4)).

$$\frac{\text{pgSi}}{\text{cell}} = \frac{\left(\frac{\text{pmolSi}}{mL}(\text{t=start}) - \frac{\text{pmolSi}}{mL}(\text{t=final})\right)}{\left(\frac{\text{cells}}{mL}(\text{t=final}) - \frac{\text{cells}}{mL}(\text{t=start})\right)} \cdot \text{M}_{Si}\left(\frac{g}{mol}\right) \tag{2.4}$$

pH The pH of the culture medium was measured using a Mettler Toledo MP 220 pH-meter. Unfiltered samples were used for the measurements. The pH of a solution is an indication of the concentration of dissolved carbon dioxide in the medium, and it is therefore an important parameter to assess not only because most diatoms have an optimum pH in which they have the highest growth rate, but also because the content of dissolved carbon dioxide is the primary carbon source for diatoms.

Instantaneous chlorophyll fluorescence (F_t) The instantaneous chlorophyll fluorescence was measured using a fluorometer (AquaPen AP 100 Photon Systems Instrument

fluorometer). This measurement gives an indication of the amount of chlorophyll present in a culture, and is therefore an efficient way of monitoring the culture development. The instrument measures photosynthetic parameters by exposing the cultures with flashes of blue light and reading the signals by a probe. An unfiltered culture sample was placed in a cuvette (Poly-methyl methacrylate, 10 mm x 10 mm disposable cuvettes with four transparent sides, Kartell) and dark-adapted for one minute before measurement. The value of *in vivo* instantaneous fluorescence was the average of six readings.

Quantum yield ($\mathbf{Q_Y}$) The quantum yield was measured by the AquaPen (see above). This parameter is a measure of the photosystem II-efficiency, which specifically gives an indication of how much of the incident light is being absorbed by the photosystems and converted to energy [3]. The fluorometer flashes the algal culture with light of a specific intensity and measures the amount of light absorbed by the photosystem. It then gives out a value between zero and one, where one is total absorption and zero is no absorption. The unfiltered algae sample was placed in a cuvette as previously described, and dark adapted for one minute before the measurement.

Macronutrient concentration Concentrations of the macronutrients, dSi, PO_4^{3-} and NO_2^- in the culture and feed media were quantified using MERCK Spectroquant test kits and a spectrophotometer (Spectroquant Pharo 100 MERCK). In this procedure an amount of sample is added different reagents that through chemical reactions create a color change whose light absorbance is measured in the spectrophotometer and converted into concentration of the measured nutrient-species. The appropriate amount of culture sample was filtered through a 0.2 µm syringe filter to which kit reagents where added following the instructions. The correct wavelength and cuvette size was set by inserting a barcoded chip into the spectrophotometer. The detection limits were 0,2 µmol/L for dSi, 6 µmol/L for NO_2^-, and 0,5 µmol/L for PO_4^{3-}.

Culture filtration Zn uptake assay samples were filtered through a 1225 Millipore sampling manifold connected to a vacuum-pump as shown in Figure 2.3. In order to decrease the possibility of metal contamination we replaced the glass tubes in the filtrate collectors with 15 mL metal free polystyrene centrifuge tubes (VWR). The polystyrene tubes were pre-weighed for accurate volume measurements after the filtration. 0.45 µm hydrophilic polyethersulfone membrane filters (Poll Life Sciences) were used for the sample filtration. The small pore size enabled the retention of both algae and bacterial species. All equipment, apart from the membrane filters and centrifuge tubes, was acid washed in a 10 % hydrochloric acid solution for several days and rinsed with Milli-Q water before use.

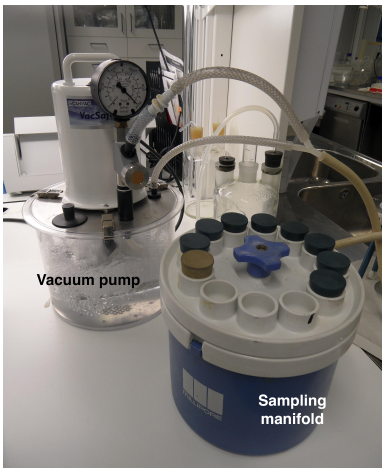

Figure 2.3: The filtration mannifold and vacuum pump

Frustule isolation and cleaning For frustule structural and elemental analysis a cleaning method that removes all organic substances within and outside the frustule is a prerequisite to obtain good results. Due to the various steps required to obtain clean frustules the reproducibility of these washing procedures is normally low. Two different cleaning methods were used; a "harsh" method using hydrogen peroxide (H_2O_2, 30 wt%), and a "soft" method using SDS/EDTA. The cleaning with H_2O_2 followed the procedure described by Townley *et al.* (2008) but with a reduction in the reaction time to 1-2 hours [76]. A schematic description of the SDS/EDTA cleaning procedure is outlined in Figure 2.4.

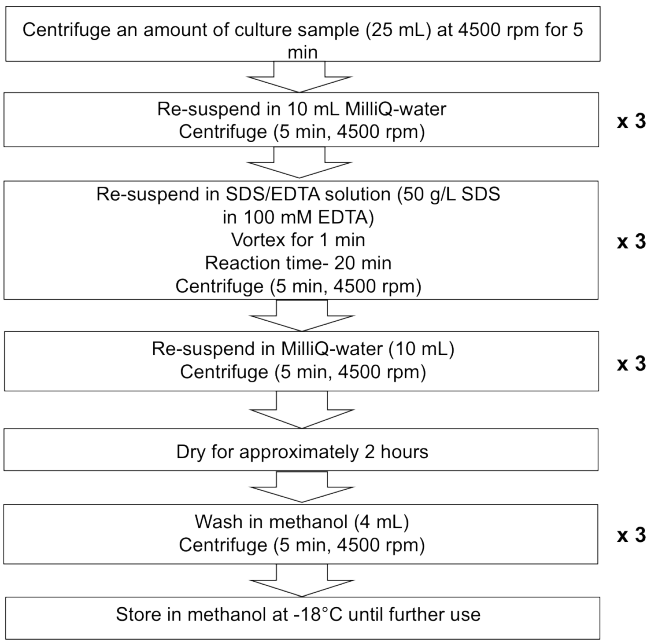

Figure 2.4: SDS/EDTA frustule cleaning method

Zn concentration in medium, organic material, and frustule Inductively Coupled Plasma Mass Spectrometry (ICP-MS) was used for compositional analysis of organic

material, filtered medium and cleaned frustules. ICP-MS is a powerful tool for compositional analysis of various materials, both liquid and solid. It combines two analytical techniques, namely inductively coupled plasma (ICP) and mass spectrometry (MS). The sample must be in liquid form to be analyzed, and solid samples are therefore digested by strong acids before they are introduced to the instrument. An argon laser decomposes the sample into neutral elements which are analyzed in the MS by means of the mass-to charge ratio of the elements [91]. The pre-treatment of the uptake assay filter samples involved a digestion step and a dilution step. The digestion included dissolution of the filters in nitric acid (HNO_3, 50 wt%) and autoclaving for approximately 1 h following a pre-determined temperature profile. Filtrate samples stored in 15 mL metal free centrifuge tubes were added HNO_3 and diluted (x10) with Milli-Q water. Frustules, washed with either SDS/EDTA or H_2O_2 cleaning method and stored in 15 mL metal free centrifuge tubes were digested in a mixture of 3+1 parts concentrated HNO_3 and hydrofluoric acid (HF) at room temperature. The digested samples were then diluted with Milli-Q water. Appropriate blanks of chemicals and equipment used for sample storage and preparation were analyzed and accounted for in the final results. Two replicate filters with corresponding filtrates from time points 0, 30, 60, 24 h, and 48 h where analysed, and the reported value is the average of the results from these parallels. For the rest of the time points only one parallel was analyzed. Each sample was run three times through the ICP-MS and the average value is reported.

Sea water chemical composition The chemical composition of sea water and experimental medium was determined by ICP-MS (see above).

Organic C/N-content The organic carbon content was used as a measure of the total biomass of the algal culture during the experiments. The carbon and nitrogen analysis was performed using a Carlo-Erba CHN+O/S elemental analyzer. These are popular and much used systems in which high temperature oxidative combustion of samples with sequential purification and separation of gases is coupled with a final chromatographic step for the identification and quantification of the elements in the sample [16]. Triplicate aliquots (10 mL) of algal culture were filtered onto pre-combusted GF/F glass fiber filters yielding circular spots of 1,1 cm in diameter. The filters were stored in the freezer until the end of the experiment. At the time of analysis inorganic carbon and nitrogen was removed by treating the filters with steaming hydrochloric acid after which they were dried in a heating cabinet at 60 °C for 2-5 min. The post-treated filters were wrapped inside a tin capsule and dried at 60 °C for 48 hours before the C/N-analysis was performed yielding the final C and N content in the capsules as μgC capsule^{-1} and μgN capsule^{-1} , respectively. For the calculation of the C and N content per mL of filtrated sample equation equation (2.5) was utilized:

$$\frac{\mu\text{g C (N)}}{\text{mL}} = \frac{\mu\text{g C (N)}}{\text{capsule}} \cdot \frac{\text{area of sample on filter}}{\text{area of bored out filter}} \cdot \frac{1}{\text{volume of sample [mL]}} \tag{2.5}$$

Frustule structure and elemental composition A Transmission Electron Microscopy (TEM) and a Scanning Electron Microscopy (SEM) were applied to examine the structure of the diatom frustules. In these methods an electron gun generates a beam of electrons that is focused by a series of lenses to form an image of the electron source at the specimen

[52]. The difference between each technique lies within the source of image generation. The TEM uses the modified post-sample electron beam to form the image, while the SEM image is formed from the backscattered electrons or the secondary electrons. For small and sensitive samples gold or carbon coating is often required to prevent charging effects induced by the electron beam. The drawback of such coating is the reduced detail resolution of the sample. The elemental composition of the frustules was investigated through the use of Energy Dispersive X-ray Spectroscopy (EDS) (Jeol 2010 F and Jamp-9500 F). The working principles for the EDS is the detection of X-rays generated by the interaction between an electron beam and a few atomic layers at a sample surface [82]. The sensitivity of the EDS is not as high as with ICP-MS, but it provides information about the relative distribution and location of the elements in the sample. A small amount of cleaned diatom frustules suspended in methanol was placed on a copper or titanium grid covered with perforated carbon film and left to dry. The sample was then mounted on a handle and positioned inside the EDS-S(T)EM for analysis.

3 Results

3.1 Culture development

The average values for the silicate content per cell reported for the preparation cultures were 1.5 and 1.23 pg Si cell^{-1} for Exp1.HD (HD='High Dose') and Exp2.LD (LD='Low Dose'), respectively. The μ_{max} for the preparation culture grown in full f/2 medium was found to be 1.15 d^{-1} with a generation time of 1.66 d^{-1}.

3.1.1 Preparation culture development

The dilution rate (D) of the exponential fed batch cultures was set at 0.03 h^{-1}. The development in the exponential fed batch cultures was followed daily for 4 weeks prior to the onset of the experiments until the optical density had stabilized. Figure 3.1 (A)-(D) shows the development in fluorescence parameters, optical density and dissolved silicate for the preparation cultures, here named Prep.Exp1.HD and Prep.Exp2.LD. Both preparation cultures where characterized by high Q_Y values which remained stable throughout the preparation time despite dSi-deplete conditions. It took about 10 days to reach steady state, judged by OD and Ft, with growth rate (0.03 h^{-1}) equal to the dilution rate (μ=D). During the whole preparation time there were excess levels of PO_4^{-3} and NO_2^- in the algal cultures.

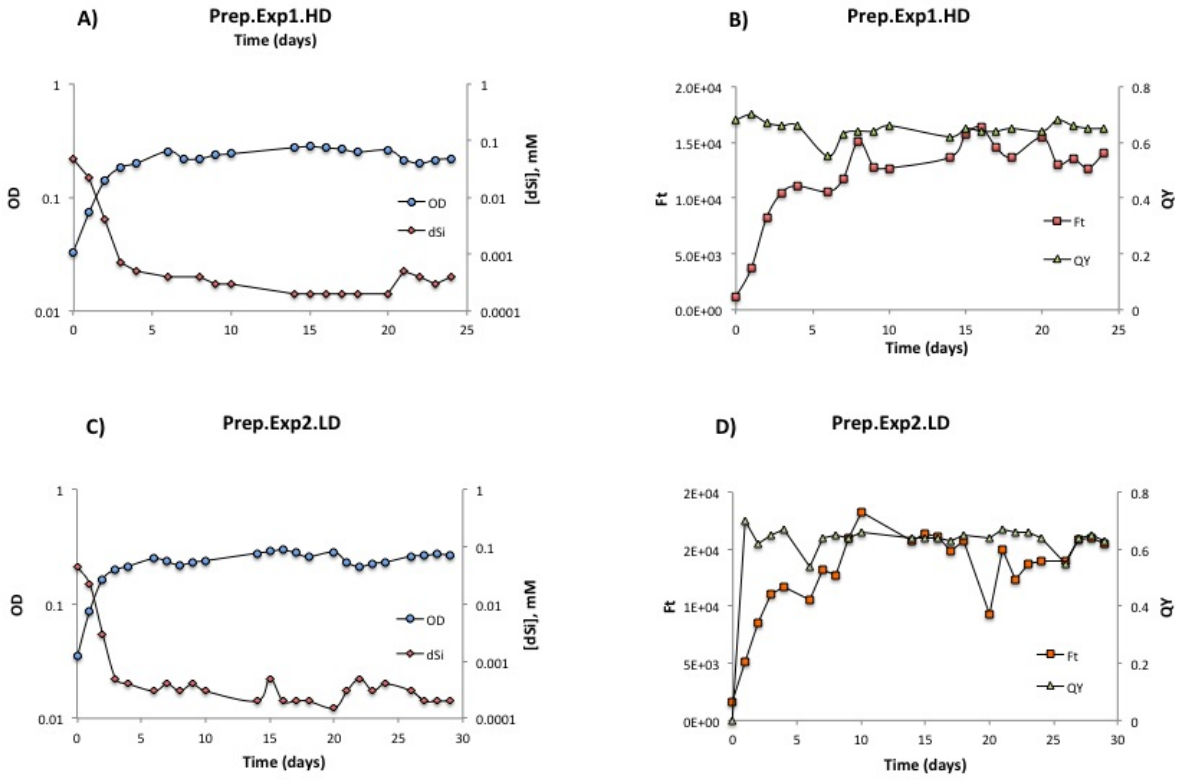

Figure 3.1: Preparation culture development; Prep.Exp1.HD (A) optical density and dSi concentration, and (B) fluorescence parameters; Prep.Exp2.LD (C) optical density and dSi concentration, and (D) fluorescence parameters. In (A) and (C) the y-axis is log-transformed.

3.1.2 Experimental culture development

Due to an underestimation of the time required for each sample to completely run through the filter there was a timeshift relative to the pre-determined time points during the first 15 minutes. Table 3.1 shows the pre-determined time points and the actual times taken for the culture to completely run through the filter in both experiments and the control experiment. The times presented are the average value of the triplicate filtrations. In the following the samples from both experiments and control will be given names according to the pre-determined time points; Exp1.HD.2 for experiment 1 timepoint 2 min, Exp2.LD.24h for experiment 2 timepoint 24 h, CM.0 for control timepoint 0, etc..

Table 3.1: Sample names and sampling times for both experiments and control experiment. All time points are in minutes unless otherwise specified.

Exp1.HD		**Exp2.LD**		**CM**	
Sample	Sampling point	Sample	Sampling point	Sample	Sampling point
Exp1.HD.Pre0	0	Exp2.LD.Pre0	0	CM.0	1.6
Exp1.HD.0	2.03	Exp2.LD.0	2.1	CM.30	31.75
Exp1.HD.2	4.09	Exp2.LD.2	3.78	CM.60	60.13
Exp1.HD.4	5.62	Exp2.LD.4	5.73	CM.24h	24.01 h
Exp1.HD.8	9.16	Exp2.LD.8	8.86	CM.48h	48.01 h
Exp1.HD.15	16.99	Exp2.LD.15	17.32		
Exp1.HD.30	30.52	Exp2.LD.30	30.58		
Exp1.HD.60	60.66	Exp2.LD.60	61.09		
Exp1.HD.24h	24.01 h	Exp2.LD.3h	3.00		
Exp1.HD.48h	48.02 h	Exp2.LD.6h	5.95		
Exp1.HD.B	-	Exp2.LD.24h	24.00 h		
Exp1.HD. frustules.24h	24 h	Exp2.LD.48h	48.02 h		
Exp1.HD. frustules.48h	48 h	Exp2.LD. frustules.24h	24 h		
		Exp2.LD. frustules.48h	48 h		

F_t and Q_Y Figure 3.2 (A) and (B) show the fluorescence development in the experimental cultures. Both cultures were characterized by having high initial photo-physiological parameters indicating that the photosystems were in good conditions. The Q_Y and F_t were assessed at more time points in Exp2.LD explaining the higher resolution in Figure 3.2 (B). The increasing trend of F_t during the experiments reflects algae growth and division. Some oscillation in the F_t were observed in experiment 2. The decrease in Q_Y and F_t between the 'pre-zero' sample and the first measured sampling point, observed in both experiments and as emphasized in the graph-enlargement in Figure 3.2 (B), is assigned partially to the time interval between the 'pre-zero' sample and the initiation of experiments but also due to a response from the additions of the silicate and zinc stock solutions. A gradual increase in Q_Y during the first 6 h was observed in experiment 2.

After 24 h the Q_Y in experiment 1 and 2 had decreased by 22% and 37%, respectively. By the end of the experiments the values showed a slight increase and the final reductions from the initial value were 21% and 29% in experiment 1 and 2, respectively.

Nutrients (PO_4^{-3} and NO_2^-) and pH development The pH and nutrient development are presented in Figure 3.2 (C) and (D), respectively. During the last 24 h of the experiments the phosphate in both cultures was depleted, indicating that the cells had taken up most of the present reserves of phosphate to accommodate growth and division. The pH in the medium increased rapidly after the addition of silicate and zinc, indicating high photosynthetic activity in the cells, and remained above 9 during the first 24 h in both experiments. By the end of the experiments the pH of the medium had again decreased to the initial values. As can be seen from Figure 3.2 (C), experiment 2 was characterized by having a higher initial and maximal pH-value than experiment 1. This is probably connected with the larger initial and final cell density of this culture.

Cell density and C and N development Linear regression was used to determine the cell density and organic carbon content (μgC mL^{-1}) for the sampling points at which these variables were not measured. Table 3.2 shows the equation parameters from the linear regression along with the correlation coefficient (R^2). Both measured and calculated values were used in the calculations and graphical presentations of the results. To test the strength of the linear regressions, data from both experiments were put together and regressions were made between carbon content, optical density and cell density. All regressions showed good correlations ($R^2 > 0.9$) (data not shown).

Table 3.2: Equation parameters from linear regressions

Experiment	Regression	Intercept	Slope	R^2
Exp1.HD	μgC mL^{-1}vs time	18.39	0.56	1.00
	cells mL^{-1}vs μgC mL^{-1}	$-1.53 \cdot 10^5$	$5.62 \cdot 10^4$	0.99
Exp2.LD	μgC mL^{-1}vs OD	5.91	58.39	1.00
	cells mL^{-1}vs OD	$2.38 \cdot 10^5$	$4.28 \cdot 10^6$	0.93

As shown by the cell development in Figure 3.3 (A) both experimental cultures had an initial stationary phase during the first hour followed by a sharp increase in cell number. The cell culture in Exp2.LD attained stationary phase between 24 h and 48 h after the initiation of the experiment, while the Exp1.HD culture did not reach this phase. After 24 h the cell number in Exp1.HD (see Figure 3.3 (A)) had approximately doubled, and by the end of this experiment the final cell number in this culture was 2.7 times the initial value. After 48 h the cell number in Exp2.LD had only increased by 1.85 times its initial value indicating that the applied dSi concentration in the medium was underestimated. The cellular organic carbon and nitrogen content (Figure 3.3 (B)) remained constant during the first 60 min in both experiments. Between 60 min and 48 h the development in Exp1.HD showed a slightly decreasing trend. Experiment 2 showed more or less constant values in the C and N development during the first 24 h, while between 24 h and 48 h there was an increase in the cellular C and N. The maximum cell specific growth rates in the experimental cultures were calculated according to the method explained in Subsection 2.5 and are shown in table 3.3.

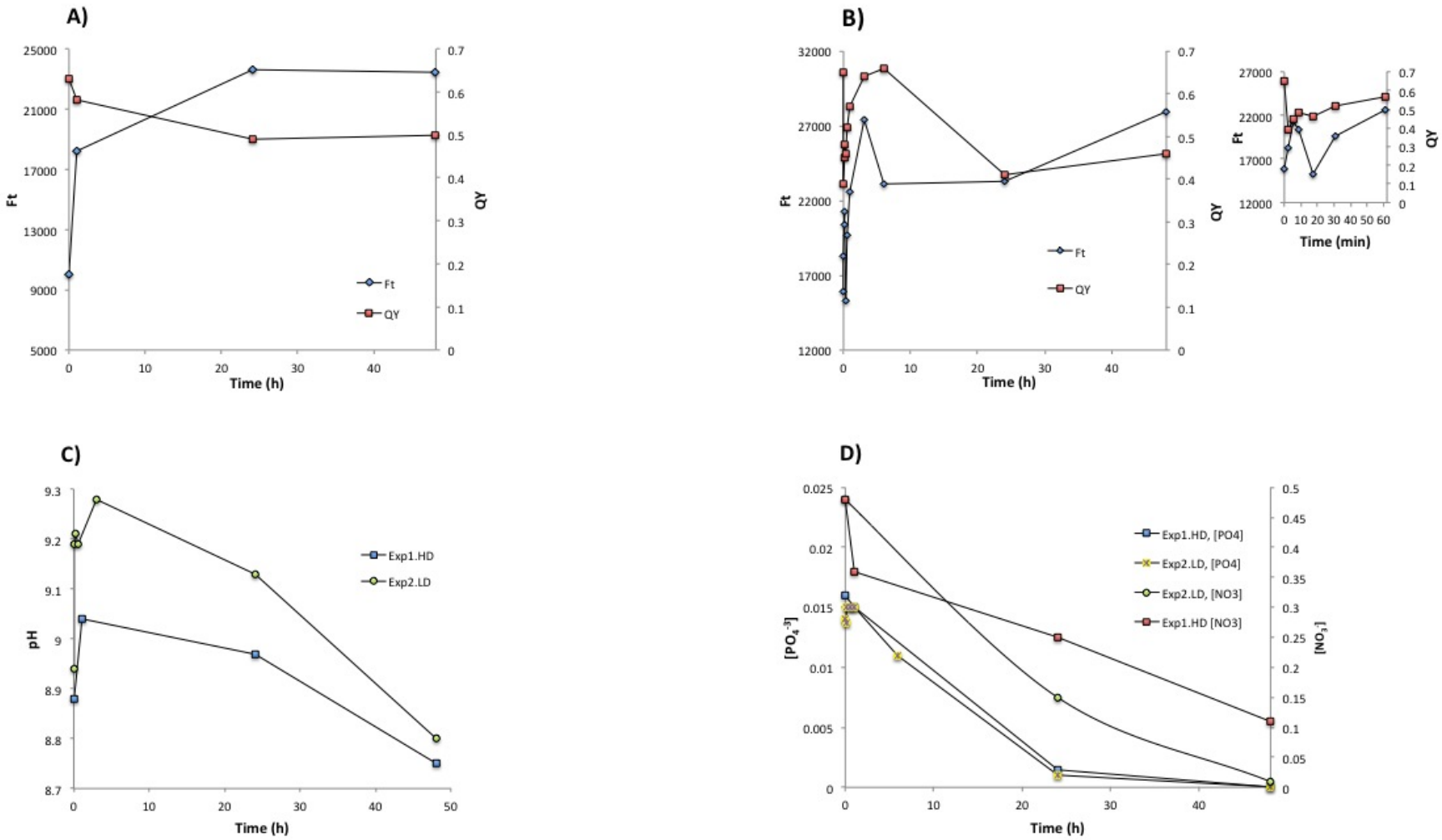

Figure 3.2: The F_t and Q_Y development in (A) Exp1.HD and (B) Exp2.LD. pH (C) , and nutrient (D) development in experimental cultures.

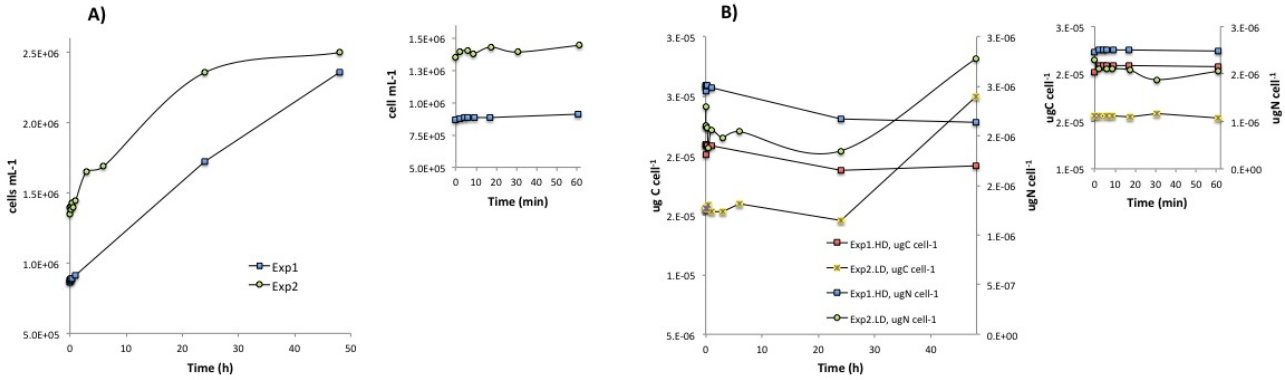

Figure 3.3: Development in (A) Cell number and (B) C and N per cell in experimental cultures. Left panels show the whole experimental period of 48 h, while inserted panels show detail of the first hour.

Morphological appearance Through inspections with light microscopy some differences with respect to size and degree of agglomeration in the *T.pseudonana* cells for the various time points were the only alterations that could be observed in the experimental cultures. For instance, the cells in the Exp1.HD.30 and the Exp2.LD.3h samples were much smaller compared with cells from other time points. It was also observed a higher amount of clustered cells in the Exp2.LD.48h sample than in the corresponding sample from the other experiment.

3.2 Zn and Si development in experimental culture

The following results presents the ICP-MS analysis of the dissolved and cellular silicate and Zn fraction development for Exp1.HD and Exp2.LD. To evaluate the consistency of Zn during the experiments the average of the sum of Zn-fraction detected in the filters and filtrates was calculated. The resulting values correlated well with the calculated Zn concentrations, indicating that no significant fraction of the metal was lost as precipitate on the walls or bottom of the culture flasks (see A, table A.7 and Figure A.1)

Medium Si and Zn development The dissolved silicate development in the culture can be seen in Figure 3.4 (A) for Exp1.HD and Exp2.LD (for raw data see A table A.2 and table A.5). Also included in Figure 3.4 is the result from the control experiment. In both experiments the dSi concentration decreased due to the uptake and growth of diatoms. Large initial decrease in the concentration indicate high adsorption of silicate to functional sites on the cellular surface followed by uptake and replenishment of cytoplasmic silicate pools. By the end of the experiments the silicate was nearly depleted from the medium with only trace amounts present (see table 3.3). The dissolved Zn concentration had an increasing trend throughout the experiments characterized by high initial increase with a gradual leveling off in the final samples (Figure 3.4 (B) with control included). A slight decrease in the metal concentration was observed for experiment 1 between the 24 h and 48 h sample. The control without cells was more stable in dZn.

Cellular Si and Zn development What here is referred to as the cellular Si and Zn concentration is the element concentrations measured in the filter samples. No distinction was therefore made between loosely and firmly bound external Si or Zn, and internal (cytoplasmic) Si or Zn (see A, table A.1 and table A.4 for raw data). This is due to the fact that the filters were not post-treated by means of a SDS-wash or trace-metal free seawater to get rid of loosely bound elements from the cellular surface as applied in other studies [88, 14]. The silicate per cell development showed an initial rapid adsorption followed by cellular uptake during approximately 10 min after the Si and Zn additions. A rapid decrease followed until approximately 17 min, after which the concentrations remained more or less constant apart from a slight decrease between 24 h and 48 h. The average uptake rate of silicate was calculated as described in section 2.5 and is presented in table 3.4.

The sorption process of Zn onto the cells (Figure 3.4 (D)) showed two phases. The first phase, representing the first 6 minutes in both experiments, was characterized by a rapid binding of Zn to the cells. At this point approximately 59% and 69% of the initial Zn added to the medium was associated with the cells in Exp1.HD and Exp2.LD, respectively. In the second phase there was quick loss of Zn from the cells, which continued for approximately 24 h. There it leveled out and finally had a slight increase between 24 h and 48 h. After 48 h, 9% and 13% of the initial Zn added to the medium was associated with the cells in Exp1.HD and Exp2.LD, respectively. The final cell-based Zn concentrations were $3.3{\cdot}10^{-4}$ and $8.8{\cdot}10^{-5}$ pmol Zn cell^{-1}, representing an increase of 84.1% and 57.5% relative to the initial cell-based concentration calculated for the 'Pre-zero'-sample for Exp1.HD and Exp2.LD, respectively. This corresponded to a 75.7% difference between the two experiments. Only the average uptake rate (equation (2.3)) of Zn by the cells could be calculated since only the first an last datapoint could be used (see table 3.4). The estimated silicate per cell content along with elemental concentrations in the culture medium of dSi and Zn after 24 h and 48 h are shown in table 3.3.

Control experiment For the control experiment only the filtrate samples were analysed. The dSi and dZn development showed stable values throughout the experimental time, indicating that the trends observed in Exp1.HD and Exp2.LD were due to the presence of cells. The average Zn concentration calculated from the filtrate results, was within ±7% of the initial concentration (see A A.8). The average dSi concentration calculated from the filtrate results, where less than ±5% different from the initial value.

Table 3.4: Meaused final cell-and Si-associated Zn, and calculated average Zn-uptake rates.

Experiment	**Measured final pmol Zn cell^{-1}**	**Measured μmol Zn mol Si^{-1}**	**Average Zn-uptake rates, fmol Zn cell^{-1} day^{-1}**
Exp1.HD	$3.31{\cdot}10^{-4}$	2817.67	0.14
Exp2.LD	$8.76{\cdot}10^{-5}$	685.80	0.03

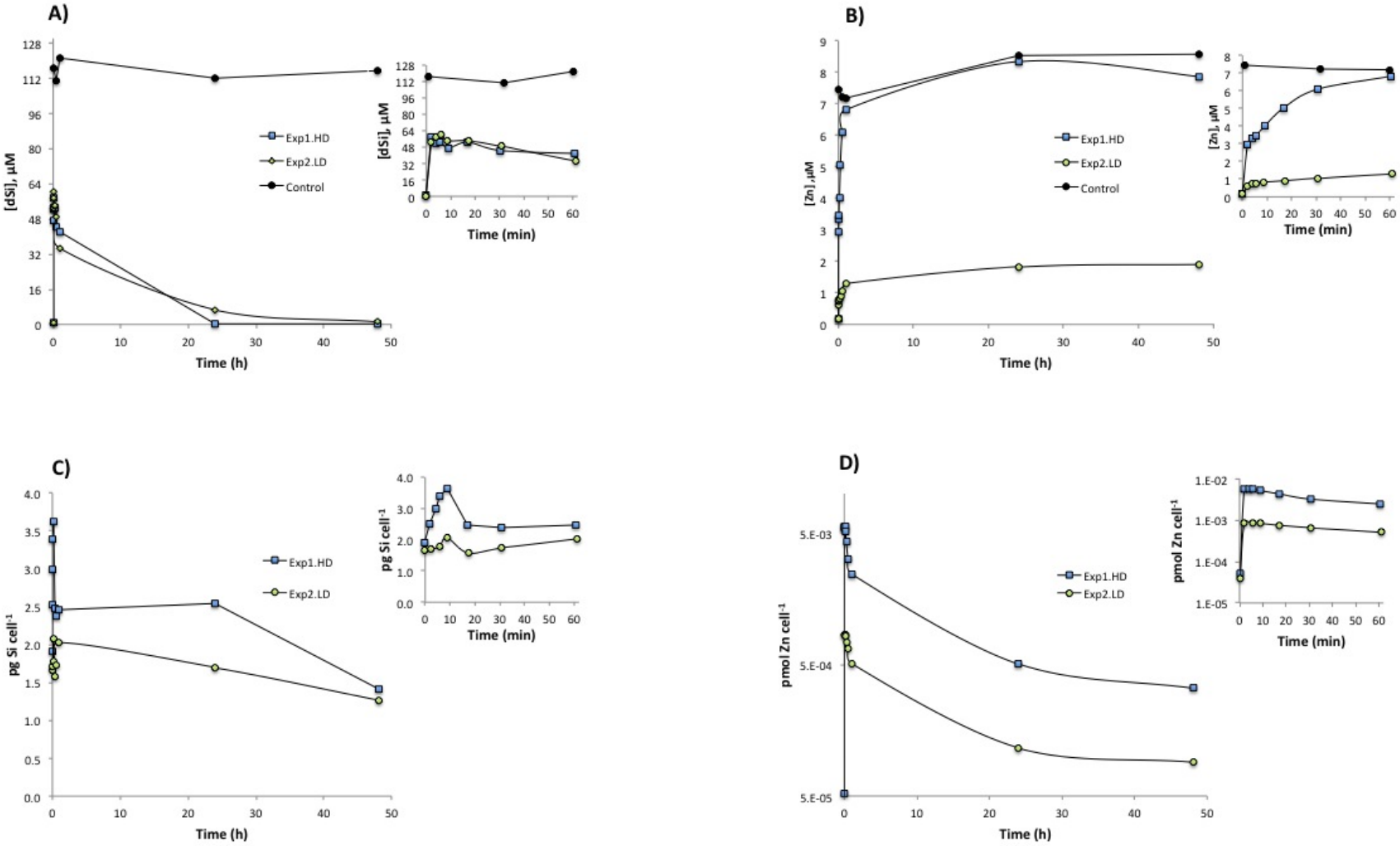

Figure 3.4: Development in dSi and Zn in dissolved ((A) and (B)) and cellular ((C) and (D)) fractions. The element concentration on the filters are converted to a per cell basis. The y-axis in (D) is log-transformed. The small plots are enlargements of the first hour.

Table 3.3: Results from the two Zn uptake studies Exp1.HD and Exp2.LD

Experiment	**Final cell number, mL^{-1}**	**$[dSi]_{medium}$ after 24 hours, µM**	**$[dSi]_{medium}$ after 48 hours, µM**	**$[Zn]_{medium}$ after 24 hours, µM**	**$[Zn]_{medium}$ after 48 hours, µM**	**Est. $\frac{pgSi}{cell}$ after 48 hours**	**Calc. μ_{max}, d^{-1}**	**Average Si-uptake rate, $\frac{pgSi}{cell \cdot h}$**	**Max Si-uptake rate, $\frac{pgSi}{cell \cdot h}$**
Exp1.HD	$2.36 \cdot 10^6$	0.30*	0.15*	8.35	7.87	1.4	1.76	0.023	11.4
Exp2.LD	$2.5 \cdot 10^6$	6.7	1.2	1.83	1.90	1.3	1.62	0.029	2.61

*Spectrophotometric results used due to negative ICP-MS values

3.2.1 Frustule elemental composition

In the following results will be presented the ICP-MS analysis of control and experimental frustules. All the results are connected to a relative standard deviation (RSD, %) (for raw data and RSD see tables A.3, A.6 and A.10 for experiment 1, 2 and control, respectively). The untreated frustules were meant to act as a reference to the experimental frustules and the results from the analysis of these frustules will be presented first. Contrary to the experimental frustules these were suspended in methanol. To assess the metal contribution from the methanol solution in the control frustules, an amount of methanol, representing the approximate amount the control frustules were suspended in, was analyzed by ICP-MS. Each control sample was analyzed two times in the ICP-MS. For the fractional calculations the average values were used. The results from the analysis showed significant differences in elemental composition between the H_2O_2- and SDS/EDTA-treated frustules. The methanol analyzed contained some trace amounts of Zn, which, when subtracting from the results of the SDS/EDTA-treated frustules resulted in a negative Zn value in this sample. The quantity of methanol analyzed may therefore have been too large leading to an overestimation of the elemental contribution from methanol in the samples. Despite this it was chosen to present analysis of the blank-corrected control frustules. Table 3.5 shows weight% and fractional standard deviation (FSD, %) of selected elements relative to the detected silicate (μg metal μg Si^{-1}) for the control frustules. Elements like B, P and Ti where high for the SDS/EDTA-treated frustules compared to those treated with H_2O_2, for which the Zn and Fe concentrations where higher.

Table 3.5: Wt% (μg metal μgSi^{-1}) of elements relative to Si in untreated (control) frustules. Also presented are the fractional standard deviations (FSD, %).

Cleaning method	**Zn**	FSD, %	**P**	FSD, %	**Fe**	FSD, %	**Ti**	FSD, %	**B**	FSD, %
H_2O_2	0.02	10.6	0.085	2.6	0.126	4.1	0.008	2.2	0.021	6.4
SDS/EDTA	0*	-	1.407	3.1	0*	-	0.119	8	0.133	1.6

* Negative values

In the following are presented the results of the experimental frustules. A problem encountered during the sample preparation of the experimental frustules was uncompleted dissolution of the frustules from the 24 h and 48 h sample from Exp1.HD. After addition of nitric acid and hydrofluoric acid it was possible to detect an amount of brownish matter in the PFA-vessels. In an attempt to further dissolve the samples they were placed in an ultrasonic bath at 50 °C for 15 minutes. But even after this treatment the visible matter had not dissolved. Table 3.6 shows the weight% of elements relative to Si in the experimental frustule samples from both the 24 h and the 48 h sample in experiment 1 and 2. The 48 h sample in experiment 2 was run two times in the ICP-MS instrument, and the reported values in table 3.6 are the average of these results. The results were corrected with UC-vessel blanks. Significant differences in the elemental fractions were observed between and within the two experiments. The Exp2.LD.24h sample had the highest detected fraction of Zn, being over 35 times higher than the 48 h sample from the same experiment and over 190 times higher than the 24 h sample from experiment 1. For experiment 1 the Zn fraction for the two sampling points were essentially the same and was comparable with the amount detected in the H_2O_2-treated control samples. Comparing

the cell associated Zn:Si ratio (μmol Zn mol Si^{-1}) at the end of the 48 h experimental period (see table 3.4) with the corresponding ratios calculated from the frustule elemental analysis (108.85 μmol Zn mol Si^{-1} and 508.47 μmol Zn mol Si^{-1} for experiment 1 and 2, respectively) the amount of frustule-incorporated Zn relative to total cell-associated Zn was 3.86% and 74.14% for Exp1.HD and Exp2.LD, respectively.

Table 3.6: The table shows Wt% of elements relative to Si (μg metal μgSi^{-1}) in the experimental frustules for the 24 hour and 48 hour samples.

	Exp1.HD					**Exp2.LD**				
	Zn	P	Fe	Ti	B	Zn	P	Fe	Ti	B
24 h	0.027	0.546	0.003	0.010	0.064	5.161	0.665	0*	0.064	0*
48 h	0.025	0.980	0.034	0.009	0.054	0.140	1.170	0*	0.048	0.416

* Negative values

3.3 Frustule structure and elemental composition

When comparing experimental frustules with frustules from an untreated *T.pseudonana* culture no structural alterations caused by the Zn addition could be revealed. The frustules were characterized by having rather thin and fragile silicate shells, as indicated by their see-through appearance in the SEM pictures (Figure 3.5). However, prominent differences were observed in untreated diatom frustules cleaned with either the SDS/EDTA or H_2O_2 cleaning procedure. The SEM inspected frustules cleaned with H_2O_2 had a higher degree of disassembled or destroyed frustules, whereas the SDS/EDTA treated frustules had a higher content of fully assembled frustules. This is clearly demonstrated in Figure 3.6. In Figure 3.5 (C), 3.7 (A) and 3.6 (D) the central tubular process termed central fultoportulae can be seen (indicated by red arrows). The average diameter of the frustules (measured from the SEM pictures) was 4 μm.

Two EDS instruments were used for the surface elemental analysis of the frustules (see Section 2.5). The first was connected to a SEM and used in the analysis of the frustules from Exp2.LD.48h. The second was connected to a TEM and used in the analysis of the frustules from Exp1.HD.48h. Due to the highly agglomerated state of the cleaned frustules it proved difficult to disperse the samples sufficiently to analyse single frustules. In an attempt to break up and disperse the Exp1.HD.48h frustules, which turned out to be the most agglomerated sample, the eppendorf containing the frustules was left in a hydrosonic bath for approximately 5 minutes. The frustule samples from the two experiments were analyzed at two different time points using different grid materials. In the analysis of Exp2.LD, which was the first sample to be analyzed, the grid material consisted of copper. Due to the proximity in X-ray energy between Cu and Zn, the Cu-signal can obscure small signals of Zn. To avoid this problem a titanium grid was used in the analysis of Exp1.HD.48h frustules. In the following EDS spectra different peak positions for the same elements reflects different X-ray energy, with those of high energy positioned to the left in the spectrum.

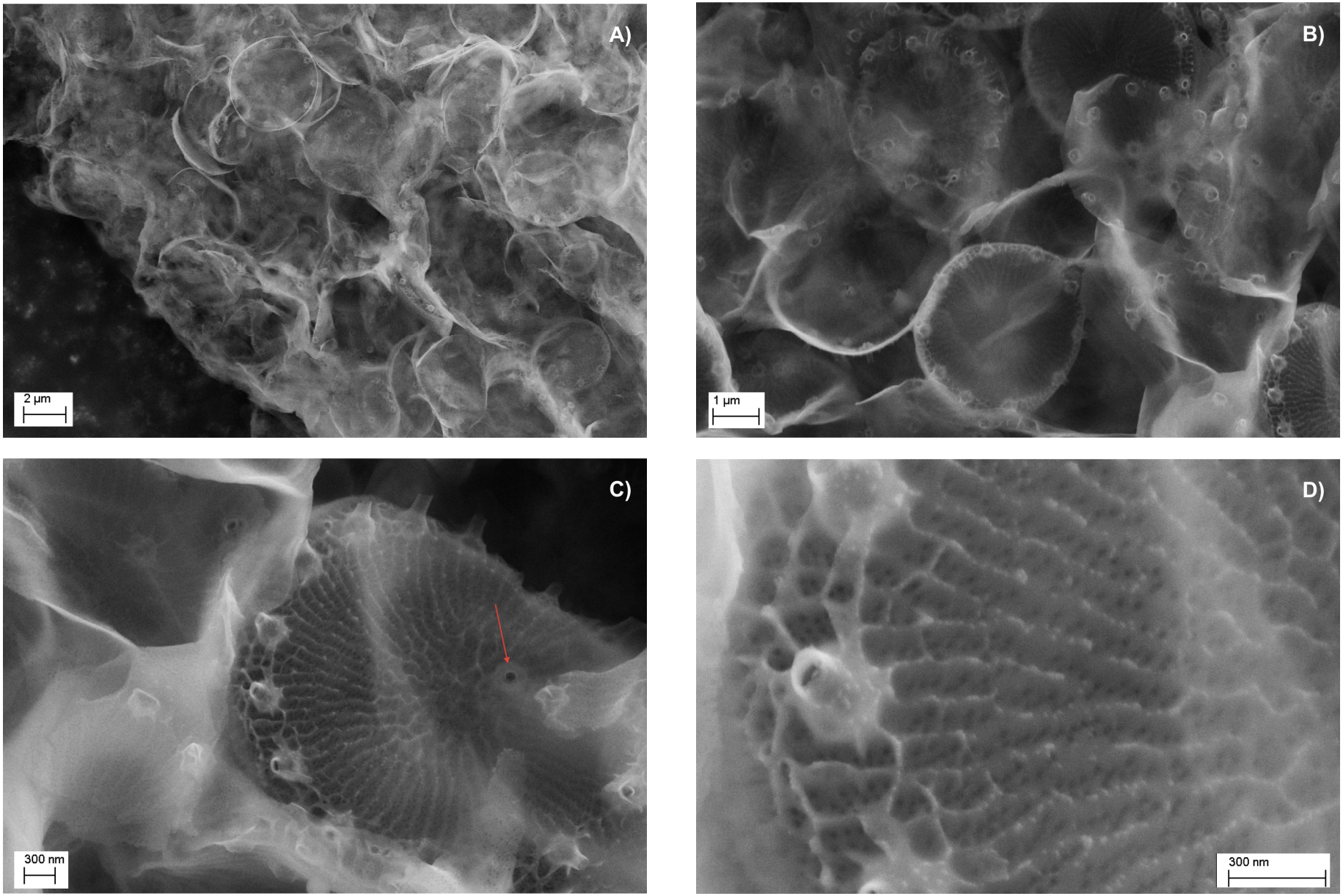

Figure 3.5: Diatom frustules from (A) Exp1.HD.24h, and (B)- (D) Exp2.LD.48h. Red arrow in (C) indicates the central fultoportulae.

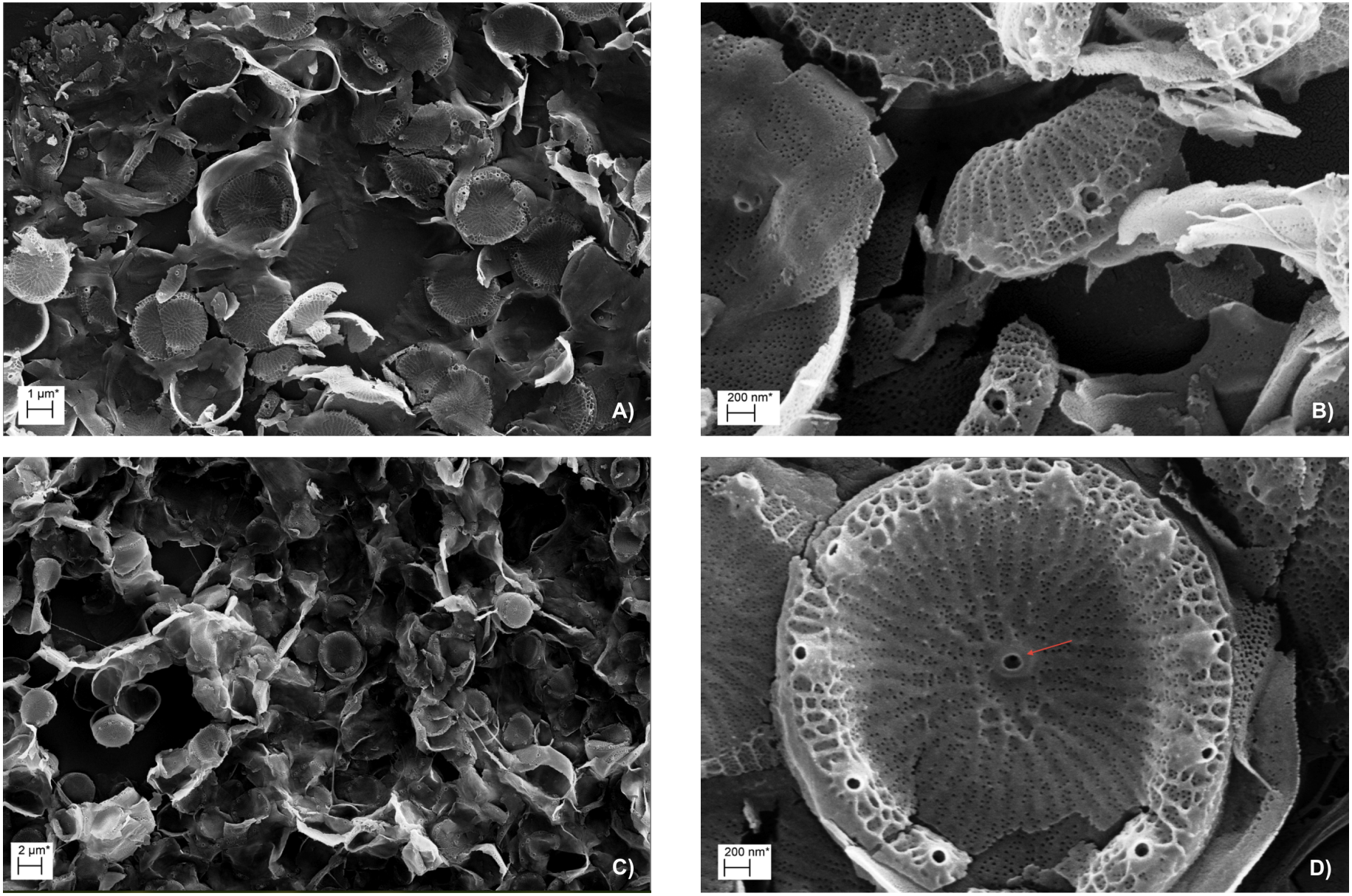

Figure 3.6: Untreated *T.pseudonana* frustules washed with H_2O_2; (A) and (B), and SDS/EDTA; (C) and (D). Higher degree of broken frustules is characterized by the H_2O_2 cleaning method. The red arrow in (D) indicate the central fultoportulae The samples have been sputtered with a nanolayer of gold to reduce charging effects.

Exp1.HD.48h Since most of the frustule layers deposited on the grid were too thick for the electrons to penetrate, most of the pictures turned out black or too obscure to see. Figure 3.7 shows the sites of analysis, which will be called site of interest Exp1.HD.1 and Exp1.HD.2 for Figure 3.7 (A) and (B), respectively. The EDS-spectrum did not reveal presence of Zn in either of the selected area (see table 3.7 for wt% of selected elements). However, when expanding an area of the spectrum between 0 and 2.6 keV from site of interest Exp1.HD.2 (insert in Figure 3.9 (B)), a peak in the area matching the X-ray energy of Zn could be seen. Due to high baseline and proximity to the X-ray energy of sodium (Na) it is unclear whether this peak represented Zn or not.

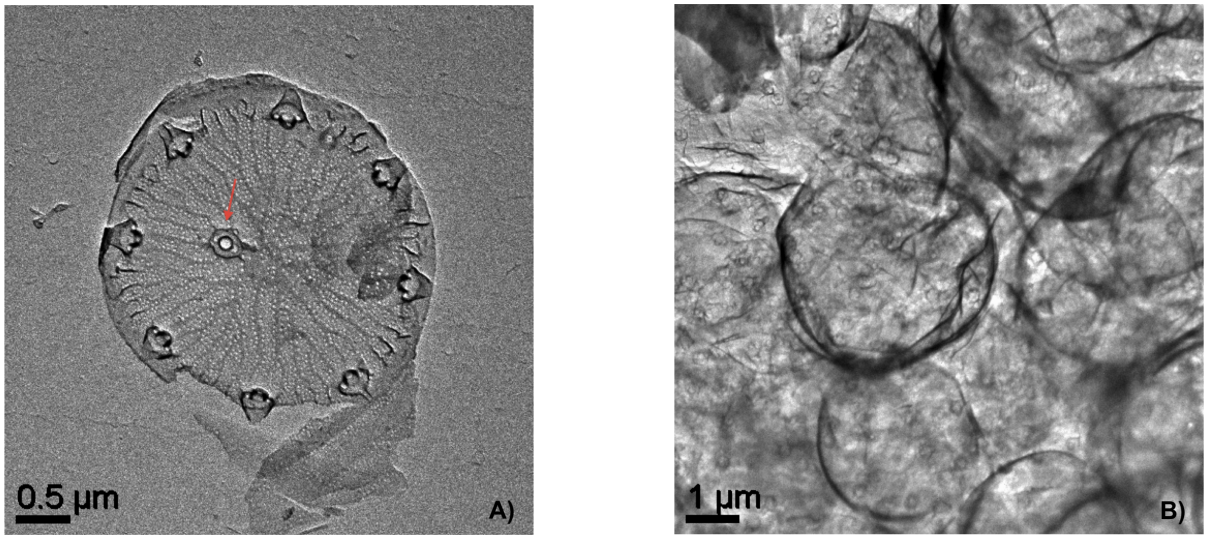

Figure 3.7: TEM pictures of selected areas for analysis. (A) site of interest Exp1.HD.1, (B) site of interest Exp1.HD.2. Red arrow in (A) indicates the central fultoportulae.

Exp2.LD.48h Figure 3.8 shows SEM-pictures taken from the Exp2.LD.48h sample. Figure 3.8 (A) clearly illustrates the high degree of agglomeration which characterized the cleaned frustule samples. The high brightness in this picture is due to charging effects from the electron beam interaction with the sample surface. Figures 3.7 (C) and (D) represent the chosen sites of interest for the EDS-analysis and will be named site of interest Exp2.LD.1 and Exp2.LD.2, respectively. When analysing singular frustules the EDS spectrum (Figure 3.9 (C)) did not reveal any peak for Zn. When analysing an area of the grid covered with a layer of diatom frustules the EDS spectrum revealed trace amounts of Zn in the order of magnitude of 0.82 wt% (see table 3.7). This is shown in Figure 3.9 (D) where the Zn-peaks are indicated by red arrows.

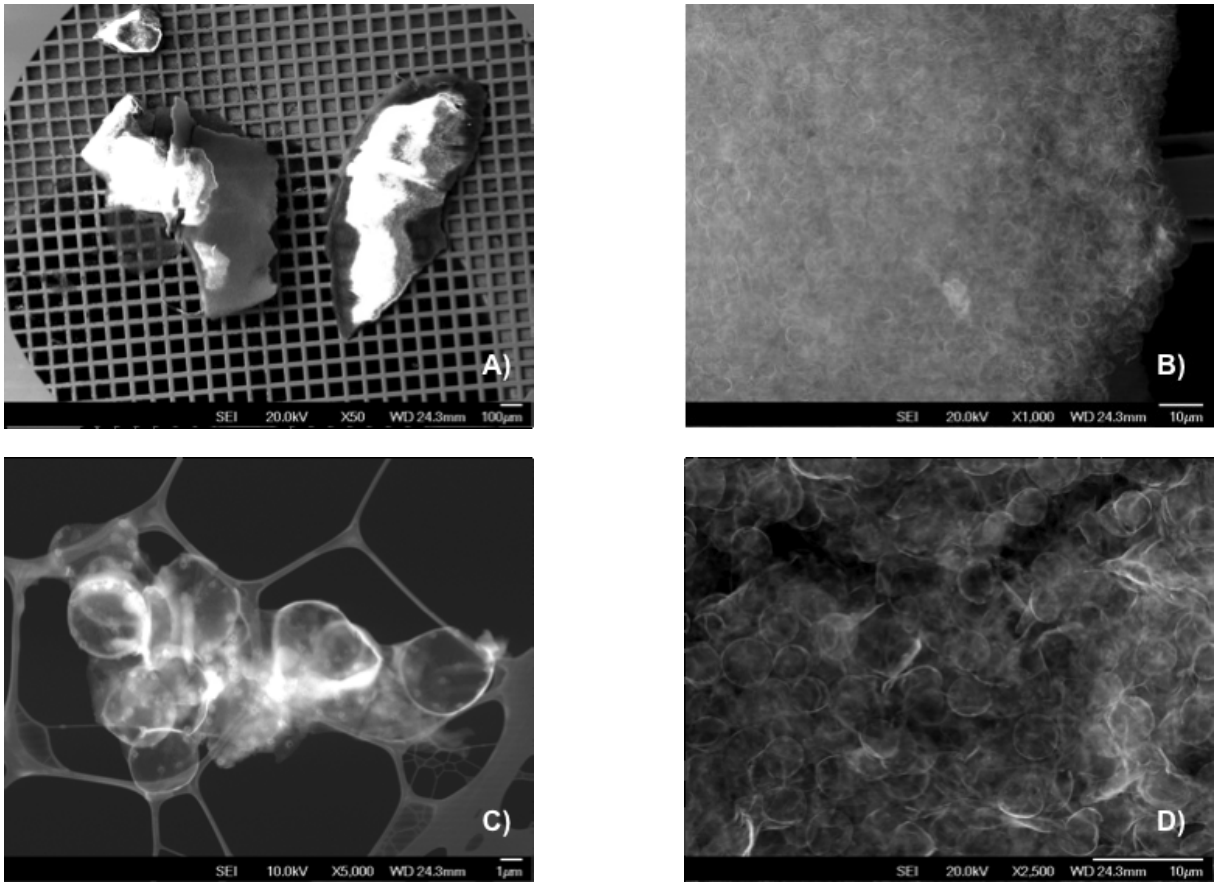

Figure 3.8: SEM pictures of frustules from Exp2.LD.48h. (C) and (D) show the sites of interest Exp2.LD.1 and Exp2.LD.2, respectively.

Table 3.7: Elements (wt%) detected with EDS in the selected sites of interest

Site of interest	**O**	**Si**	**Cl**	**Zn**
Exp1.HD.1	32.87	23.44	0.18	-
Exp1.HD.2	15.98	51.79	-	-
Exp2.LD.1	27.41	25.40	0.33	-
Exp2.LD.2	17.68	31.44	0.84	0.82

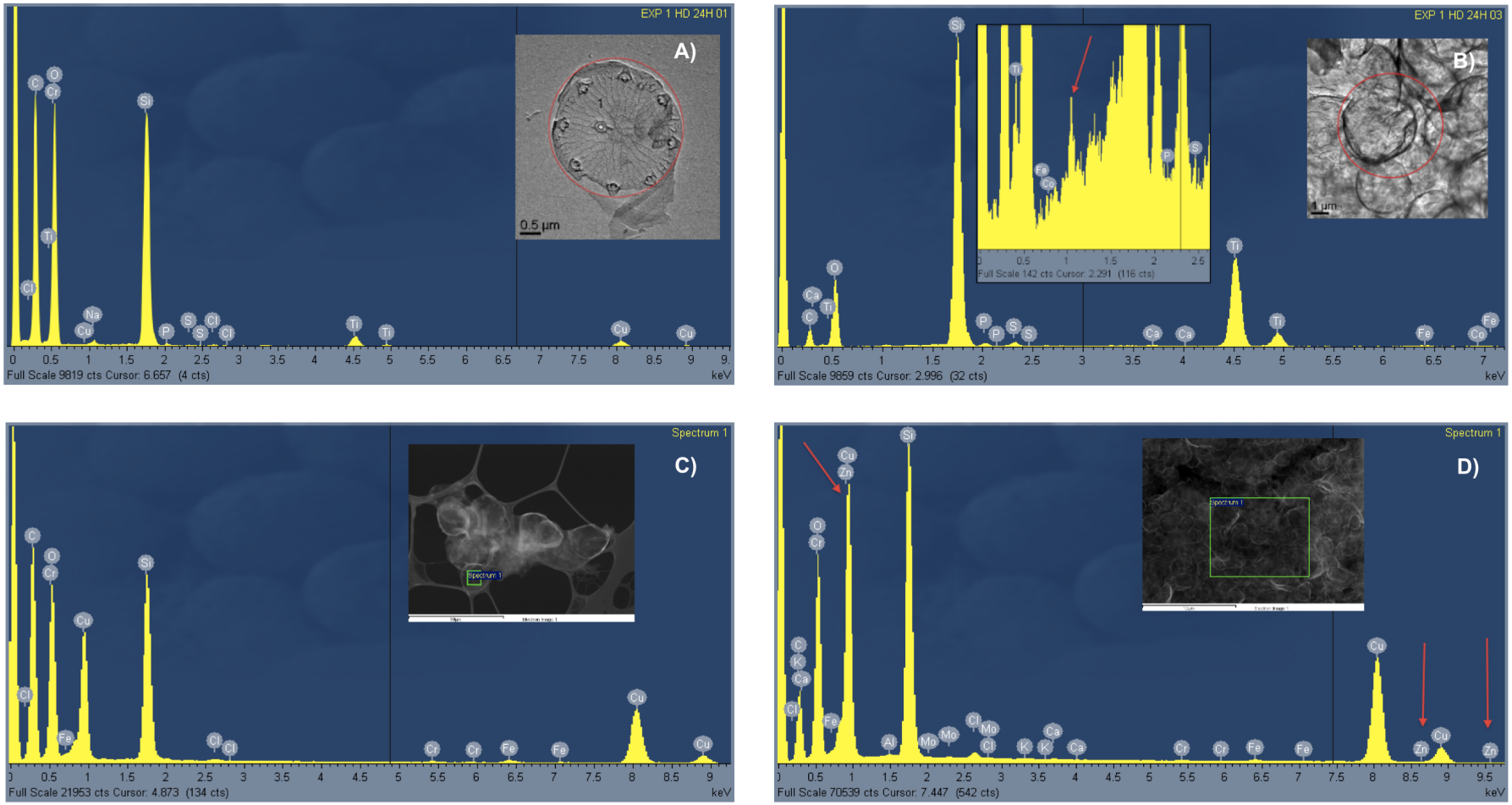

Figure 3.9: EDS spectra and S(T)EM pictures of selected site of interest for Exp1.HD: (A) single cell and (B) agglomerated cells, and Exp2.LD: (C) single cell and (D) agglomerated cells. In (B) the red arrow in the expanded area of the spectrum indicate the peak in the energy position corresponding to Zn. Red arrows in (D) indicates the position of Zn detected.

4 Discussion

This study focuses on the uptake, cellular response, and intracellular and frustule associated Zn concentration in the diatom *Thalassiosira pseudonana.* It was also our intention to perform uptake experiments in order to assess the possibility to produce Zn doped diatom frustules in an easy and reproducible way avoiding the use of, for instance, radioactive isotopes.

4.1 Culture development and response to Zn addition

The silicate per cell content calculated for the preparation cultures were in good agreement with literature data adapted from E. Paasche, 1.41 and 1.81 pg Si cell^{-1} [55, 54], and D. Werner, 0.6-1.5 pg Si cell^{-1} [85]. The photosynthetic parameters, F_t and Q_Y, as well as growth rate and silicate uptake rate are good measures of photo-physiological condition of the cells and indication of cellular stress responses. Stress can be induced by various environmental variables including nutrient depletion [44, 5], metal toxicity or metabolites present in the environment [87, 48], pH [28], temperature and light intensity [4, 87].

F_t and Q_Y Assessing the Q_Y value of a photosynthesizing algal culture gives the advantage of immediate evaluation of the cellular condition and response to toxins. The F_t and Q_Y profiles in both experiments indicated high photo-physiological conditions with some oscillations observed in experiment 2 (Figure 3.2 (B)). These initial oscillations are assigned to responses to the metal additions, increased pH, and possibly to rearrangements of chloroplasts to accommodate increased need of energy for growth and biosilicification. The increasing trend in F_t values during the first hour, as observed for experiment 2, is related to growth of cells. By the end of the experimental time both cultures showed a slight decrease in the Q_Y, reflecting a reduction of the photosystem II efficiency and that cells were in a stressed condition. Due to the constant change in variables reflecting environmental and cellular factors in batch cultures it is challenging to determine the main reasons for a decrease in physiological state. It is believed however, that the silicate depletion was the major reason to the observed decrease in the Q_Y values [44, 41]. Self-shading due to increased optical density and high metabolite production can also affect the photo-physiological condition [87, 48]. In the case of the Exp1.HD culture the much higher initial Zn concentration present in the experimental medium may also have been an external factor leading to decreasing Q_Y values. It is known that Zn may reduce photosynthetic performance through inhibition of the electron transport in Photosystem II [49, 61], but since neither the maximal growth rate nor the silicate uptake rate were severely reduced in this experiment it is unlikely that the presence of Zn has exerted major inhibition on the cells. This is consistent with the results of Fisher *et al.* (1984) [17] in which no significant reduction in growth rate was found for the Zn concentration range applied in this study. In addition it would be expected to observe a much higher decrease in the Q_Y values if acute metal stress had been imposed [48].

Nutrients The increased uptake of nutrients by the diatom cultures during the course of the experiments reflects the increased growth activity upon the silicate addition to the medium. The calculated maximal growth rates of the algal cultures indicate that the phosphate depletion of the medium did not exert any prominent affect on the cells.

This finding is consistent with the data from the study of Parslow *et al.* (1984) [57] in which the growth rate of *T. pseudonana* remained close to μ_{max} during 12 h of phosphate starvation, indicating the presence of intracellular phosphate storages.

Development in cell number and C and N content of cells The earlier onset of cell division in Exp1.HD, observed by the difference between the initial and the 24 h cell density, indicates that some cells in this culture were in late G1-or even early G2-phase of the cell cycle when the experiment was initiated. This may explain the higher increase in final cell number of this culture. In cells which grow under unlimited conditions, C and N per cell content will have doubled before binary cell division occurs [15]. The on average unchanged C and N content per cell in the experimental cultures is assumed to be connected with unsynchronized algal cultures and that cells divided independently of each other. The increase in both variables between 24 h and 48 h in experiment 2 indicates that the depletion of dSi from the medium after 24 h provided the cells with time to accumulate organic carbon and nitrogen rather than proceeding the cell division cycle, and that the cells in this culture, which did not reach a full doubling, were very near a doubling at this stage.

Visual appearance The cells in Exp2.LD.48h were characterized by a higher degree of cell-clustering than the corresponding sample from experiment 1. According to Parslow *et al.* (1984) [57] this is a normal physiological stress response induced by silicate starvation. The earlier onset of silicate depletion and the higher cell density observed in Exp2.LD may have contributed to this outcome. Structural analysis of experimental frustules did not give any indication that the added Zn had induced structural changes in pore structure or valve symmetry. It was, however, difficult to find individual frustules that could be studied in detail due to their agglomerated condition. As observed by Ellwood and Hunter (2000) [14] under Zn and Si limiting conditions the diatom *T.pseudonana* is known to become smaller in size. Judging from the size measured on basis from the attained SEM-pictures the experimental diatoms were in the lower range of the attainable diameter of this species (see Section 1.2.1). Considering that the preparation cultures were grown on Si- and Zn-deplete medium for several generations prior to the experiments, the small and thin frustules are probably reflecting diatom growth under limiting silicate availability. As observed by Paasche *et al.* (1973) [54], the amount of Si used in the frustule construction is decreased under Si-deplete conditions, which may explain the see-through appearance of the frustules in the electron microscope.

4.2 Frustule cleaning methods

The H_2O_2 method is an efficient cleaning process yielding frustules with little or no associated organic material on the frustule surface. Because of the oxidizing nature of the hydrogen peroxide the frustules often become brittle and fragile [1, 37]. The SDS/EDTA cleaning method usually leaves the frustules fully assembled and should not impose any oxidizing or dissolving effect on the frustules. These claims were confirmed through the structural analysis by SEM of frustules cleaned with either method (see figure 3.6). A higher degree of fully assembled frustule-valves was found in the SDS/EDTA cleaned frustules, whereas the frustules cleaned with the H_2O_2 procedure was branded by the oxidative nature of the chemical, making the frustules more brittle and consequently more

prone to destruction during centrifugation. A problem encountered in this study when trying to optimize frustule washing procedure was the low reproducibility of the methods. This is due to variations in sample size, physical state of the cells (high or low production of extracellular material) and other differences, which often leads to the requirement of repeating one or more steps in the cleaning procedure in order to obtain clean frustules. In addition to the above-mentioned differences in frustule condition and visual appearance, the cleaning methods resulted in frustules with substantial differences in elemental composition. In order to obtain frustules with comparable elemental constitution, a persistent cleaning method is of utmost importance.

4.3 Element surface adsorption and uptake by diatoms

Silicate The high negative slope of the concentration of dissolved Si in the medium over the first 10 minutes indicates a fast adsorption of silicate to functional sites on the cellular surfaces followed by surge uptake by the cells [5]. This is supported by the Si per cell development where an immediate Si adsorption to cell surface followed by replenishment of internal Si-pools can explain the peak in these values approximately 10 min after the addition of Si to the medium (figure 3.4 (C)). The difference in the maximal Si uptake rate was related to a higher cell density present in experiment 2 and thus lower Si added per cell. By the end of both experiments the medium was nearly depleted of dissolved Si and the trace amounts still left in the medium were assumed to represent the diffusion limiting Si concentration.

Zinc As emphasized by the control experiment, the changes in dissolved Zn concentration in the culture medium of Exp1.HD and Exp2.LD were due to the presence of cells and not caused by precipitation or adsorption to flask walls and bottom. The trend in the cell-associated Zn illustrates an adsorption-desorption equilibrium in which high initial adsorption onto cellular surfaces was followed by gradual desorption until reaching an equilibrium situation [89, 11, 34]. As the pH-profile from the experiments in this study illustrates, and as substantiated by the work of Pokrovsky *et al.* (2005) [58], the adsorption-desorption process follows a pH-dependent pattern. The high initial increase in pH may have led to temporary precipitation of Zn-hydroxides (mainly in the form of $Zn(OH)_2$ [93]) onto or around the cells. In the work of Skjåk-Bræk *et al.* (1980) [6] a similar trend in the cell-associated metal concentration was observed after addition of Zn to a culture of the diatom *Phaeodactylum tricornutum*. The author showed that below pH 9.0, 50% of the cell associated Zn was precipitated Zn. At pH values above 9.0 there was a rapid increase in the fraction of precipitated Zn. The assumed formation of particulate Zn observed in this study is substantiated by the speciation model by Zirino *et al.* (1972) [93] which states that at pH values above 9.0 almost 100% of the Zn exists as $Zn(OH)_2$. Moreover, Skjåk-Bræk *et al.* (1980) [6] postulated that the presence of cells would enhance Zn precipitation by offering surface area where particulate metal could bind. This was also shown in the work of Webb *et al.* (2000) [84] who found that biological surfaces acted as templates for the formation of zinc-rich particles. In addition, the presence of increased concentration of organic material in the medium due to excretion of exudates from actively photosynthesizing and dividing cells or as a defense mechanism towards Zn addition, may have led to increased metal complexation [18]. This is supported by the findings of Xue *et al.* (1988) [89] and Fisher *et al.* (1981) [18], which demonstrated that

certain cellular exudates could form non-labile complexes with metals and protect the cells from high levels of toxic elements. It is therefore believed that the temporary precipitation of particulate Zn (creating non-available metal species) combined with larger amounts of organically complexed Zn have prevented the cells from taking up Zn. High amounts of precipitated Zn attached to the cell surfaces may have reduced the photosynthesizing activity of the cells, leading to a decrease in the pH as observed in the cultures after approximately 6-10 h. This again may have induced the desorption and dissolution of the metal as observed in the cellular-Zn development (see Figure 3.4 (d)).

Avoiding precipitation of zinc hydroxides would require a more extensive pH control of the experimental medium, through for instance CO_2-bubbling of the culture. Another possibility would be to equilibrate the experimental medium and the added Zn solution prior to the experiments. But by transferring aliquots of algal cultures to the experimental medium additional variables concerning temperature, medium composition and pH would be introduced to the experiments. In order to get a more accurate assessment of the amount of Zn firmly bound to the cellular surfaces or present in the cytoplasm, the filters should go through a washing procedure including a chelating agent, such as EDTA, immediately after the filtration. In this way the fraction of loosely bound Zn, represented by the amount of Zn present in the EDTA solution after the washing step, could be determined. The fraction of organically complexed Zn could be determined by using different voltametric methods, such as differential pulse anodic or catodic stripping voltametry [17, 78].

Zn and silicate uptake Zn uptake rates were calculated by comparing the difference in Zn concentration as measured in the filters from the pre-zero sample and the 48 h sample divided by the increase in cell number and experimental duration in days. No distinction was therefore made between the Zn adsorbed onto the diatom surface and the Zn present in the cytoplasm, so that the actual Zn uptake rates might have been lower than those calculated in this study. Comparisons between studies are often tenuous and difficult because different studies employ different techniques, different growth media and metal concentrations, and different strains of the same algae species, which may have pronounced effect on metal sensitivity and uptake. However, the zinc uptake rates measured in this study are 10-100 times lower than the rates measured by Ellwood *et al.* (2000) [14]. The reduced concentration of free zinc ions in the medium caused by metal precipitation is probably the main reason leading to the low uptake. The surge uptake of Si observed during the first 10 minutes after Si and Zn addition were much higher than any of the literature data found on uptake rates of pre-starved *T.pseudonana* cultures [75, 30]. Again it has to be stressed that no distinction was made between adsorbed and intracellular Si, and that initial adsorption of the element onto cellular surfaces may have been misinterpreted as Si uptake, and that the actual rate of uptake was much lower. These findings are supported by the observations made by Thamatrakoln *et al.* (2008) [75], in which long-term starved cells (24 h-starvation) had a much lower content of intracellular Si-pools resulting in a lower maximal uptake rate.

4.4 Frustule elemental composition

The ICP-MS results from the analysis of frustules were difficult to interpret due to the various sources of error involved in the preparation of the samples. The experimental frustules were not suspended in methanol after the cleaning procedure, but washed several times with Milli-Q water and stored in the freezer until the ICP-MS analysis. Dissolution problems, and small sample sizes may have resulted in errors concerning the concentration of silicate and other trace metals. Also the different washing procedures introduced contamination risks as indicated in the elemental analysis of the control frustules (see Section 3.2.1 and table 3.5). The control frustules originated from the same algal culture and should theoretically have the same elemental composition, but the ICP-MS analysis showed prominent differences for some of the elements detected dependent on washing procedure. Even though the low reproducibility of the washing procedures limited the comparison of elemental quantity in frustules cleaned with either procedure, a higher sample quantity of the control frustules allowed the comparison of some of the major differences. The H_2O_2 cleaning may have had an etching effect on the frustules thus leading to the dissolution of some elements like Ti. This is consistent with other studies comparing the same cleaning procedures [33]. The H_2O_2 cleaned frustules showed the highest concentration of Zn and Fe. Contamination from the H_2O_2 solution or from trace metals originating from equipment used during the cleaning process may have led to increased Zn in the sample. EDTA is a strong chelating agent, and any contamination occurring throughout the frustule cleaning with SDS/EDTA would probably be complexed with the chelator and washed out with Milli-Q water.

The results from the experimental cultures showed significant variations in the Zn fraction detected, and in the case of experiment 2 also between the two separate sampling points (24 h and 48 h). What must be emphasized is that after division the newly synthesized frustules may contain Zn, consequently after 48 h some frustules may contain the double Zn/Si-fraction as that listed in table 3.6. The Zn/Si-ratio in the 24 h frustule sample from experiment 2 was approximately 200 times higher than the corresponding sample in experiment 1. As indicated by the control frustules much of this high difference may be associated to metal contamination from the H_2O_2 procedure used for these frustule samples. The variation between the two sampling points in experiment 2 largely emphasize the possible contamination from the cleaning. However, when comparing Exp1.HD frustules with the control frustules treated with SDS/EDTA, and Exp2.LD frustules with the control frustules treated with H_2O_2, the Zn fraction in the experimental frustules were significantly higher. Due to the higher concentration of Zn applied in experiment 1 it is probable that a higher fraction of the metal was in a particulate form compared to experiment 2. And considering that a higher fraction of added Zn was attached to cells in the final sample of experiment 2 (as calculated in section 3.2), the bioavailability and consequently the uptake of Zn may have been larger leading to the higher content of Zn measured in the frustules from this experiment. This is reflected by the final calculated value of frustule-associated Zn relative to the final cell-associated Zn for the experiment 2. The higher bioavailable Zn in experiment 2 is supported by the model of Ellwood *et al.* (2000) [14] relating the Zn-fraction (normalized to Si) in the frustule of *T.pseudonana* with ambient concentrations of free Zn^{2+}. According to this model, the free Zn^{2+} concentration in the current experiments would be in the order $10^{-8.2}$- $10^{-7.5}$ M for Exp1.HD

and Exp2.LD, respectively (48 h sample). This indicates that the calculated uptake rates of Zn, which was higher for experiment 1, have been camouflaged and consequently overestimated by high adsorption of particulate Zn onto cellular surfaces. The insignificant difference (<10%) in Zn fraction between the 24 h and 48 h frustule samples of experiment 1 indicates that the measured concentration for these frustules are more accurate.

Due to the high uncertainty around the quantitative precision around the ICP-MS frustule analysis, combined with the dissolution problems of the frustules and the uncertainties around the various contamination sources connected with the frustule cleaning, the discussion and conclusions of the metal concentration in the frustules in this study are only indicative.

4.4.1 Frustule element analysis by EDS

For the EDS element analysis of the diatom frustules only the 48 h samples from each experiment were analysed because it was assumed more probable (~50%) to locate second generation frustules here than in the 24 h frustule sample. The agglomerated state of the cleaned frustules proved to be a challenge during the grid-deposition of the sample prior to analysis, and it was difficult to find single frustules that could be analyzed. Together with the possibility that analysis was made on first generation valves, the presence of small and highly dispersed quantities of Zn in the frustules may not have been detected by the EDS scan when analyzing smaller area of the samples. However, as already discussed a higher bioavailable Zn fraction in the low dose experiment may have led to increased uptake and frustule incorporation. This was further substantiated when trace amounts of Zn were detected through EDS scan in the 48 h frustule sample from the low dose rather than the high dose experiment. Due to the small quantity of detected Zn, analysis of the metal localization in the frustule could not be performed.

5 Conclusion

The main issue standing out in this work is the complex chemistry involved between the dissolved Zn, photosynthetic activity of diatom cells, and cell surface chemistry, and how these issues together affect the bioavailability and consequently the uptake of Zn. The fluorescence parameters Q_Y and F_t were assessed to follow the photo physiological response of the cells during the experimental period. Both experiments were characterized by on average high Q_Y values indicating good photo physiological conditions. Some oscillations during the first part, as observed in experiment 2, were assigned to cellular response to Si and Zn additions and to possible rearrangements of chloroplasts to accommodate the increased need of energy for growth and biosilicification. Other than this no particular cellular response to Zn addition was detected. As shown by the cell-associated Zn and the dissolved Zn profiles, a two-phase sorption process occurred. In the first phase Zn got attached to the cellular surface through ligand-metal interactions or through chelation with organic exudates excreted from the cells, followed by a gradual metal desorption in the second phase. It is believed that the high increase in pH led to a temporary precipitation of particulate Zn onto the cells. This chemical state of Zn may have prevented cells from taking up and incorporating the metal in a quantity representative to the medium concentration. However, comparing the metal content in experimental frustules with that from untreated frustules, a higher amount of Zn in the treated frustules was revealed, indicating that increased uptake of Zn had occurred. It is believed that the increased exposure of the experimental diatom cultures to Zn may explain this observation and that it therefore is possible to produce Zn doped frustules with the desired properties for solar cell technological purposes under appropriate circumstances and under close pH control.

6 Future work

In order to accommodate the chemistry involved in the interaction between dissolved metals in seawater with algal surfaces and metabolites, and to avoid reduced metal bioavailability, it is important to obtain extensive control of the pH of the medium. For elemental composition analysis of the frustule it is important to develop a reproducible cleaning procedure that diminishes the contamination risks to a minimum. Future work should involve implementation of more uptake assays with more replicates in order to obtain sufficient data, of which statistical analysis and correlation calculations can be performed. For the study of the incorporation and production of Zn doped frustules a more efficient and controllable approach would be to grow cells in semi-continuous cultures providing a medium containing the wanted concentrations of metal over a longer time. For the study of uptake of Zn by diatoms uptake assays with and without washing procedure of filter samples may be used in order to distinguish between adsorbed and intracellular metal.

References

[1] F. Abrantes, I. Gil, C. Lopes, and M. Castro. Quantitative diatom analyses–a faster cleaning procedure. *Deep Sea Research Part I: Oceanographic Research Papers*, 52:189–198, 2005.

[2] M. B. Andersen, D. Vance, C. Archer, R. F. Anderson, M. J. Ellwood, and C. S. Allen. The Zn abundance and isotopic composition of diatom frustules, a proxy for Zn availability in ocean surface seawater. *Earth and Planetary Science Letters*, 301:137–145, 2010.

[3] AquaPen-100, Photon System Instruments. *Aquapen operation manual*.

[4] H.A. Barker. Photosynthesis in diatoms. *Archives of Microbiology*, 6:141–156, 1935.

[5] J. Beardall, E. Young, and S. Roberts. Approaches for determining phytoplankton nutrient limitation. *Aquatic science*, 63:44–69, 2001.

[6] G. S. Bræk, D. Malnes, and A. Jensen. Heavy metal tolerance of marine phytoplankton. IV. Combined effect of zinc and cadmium on growth and uptake in some marine diatoms. *Journal of Experimental Marine Biology and Ecology*, 42:39–54, 1980.

[7] M.R. Brown and K.A. Miller. The ascorbic acid content of eleven species of microalgae used in mariculture. *Journal of applied phycology*, 4:205–215, 1992.

[8] E. Brunner, C. Kröger, and K. Lutz. Analytical studies of silica biomineralization: towards an understanding of silica processing by diatoms. *Applied Microbiology and Biotechnology*, 84:607–616, 2009.

[9] E. Brunner, P. Richthammer, H. Ehrlich, S. Paasch, P. Simon, S. Ueberlein, and K.H. van Pée. Chitin-based organic networks: An integral part of cell wall biosilica in the diatom *Thalassiosira pseudonana*. *Angewandte Chemie*, 48:9724–9727, 2009.

[10] R. H. Byrne, L. R. Kump, and K. J. Cantrell. The influence of temperature and pH on trace metal speciation in seawater. *Marine Chemistry*, 25:163–181, 1988.

[11] P. G. C. Campbell, O. Errécalde, C. Fortin, V. P. HIriart-Baer, and B. Vigneault. Metal bioavailability to phytoplankton- applicability of the biotic ligand model. *Comparative Biochemistry and Physiology Part C*, 133:189–206, 2002.

[12] X. Chen and S. S. Mao. Titanium dioxide nanomaterials: Synthesis, properties, modifications, and applications. *Chemical Reviews*, 107:2891–2959, 2007.

[13] S. W. Chrisholm, F. Azam, and R. W. Eppley. Silicic Acid Incorporation in Marine Diatoms on Light:Dark Cycles: Use as an Assay for Phased Cell Division. *Limnology and Oceanography*, 23:518–529, 1978.

[14] M. J. Ellwood and K. A. Hunter. The incorporation of zinc and iron into the frustule of the marine diatom *Thalassiosira pseudonana*. *Limnology and Oceanography*, 45:1517–1524, 2000.

[15] R. W. Eppley, R.W. Holmes, and E. Paasche. Periodicity in cell division and physiological behavior of *Ditylum brightwellii*, a marine planktonic diatom, during growth in light-dark cycles. *Archiv für Mikrobiologie*, 56:305–323, 1967.

[16] V. P. Fadeeva, V. D. Tikhova, and O. N. Nikulicheva. Elemental analysis of organic compounds with the use of automated CHNS analyzers. *Journal of Analytical Chemistry*, 63:1094–1106, 2008.

[17] N. S. Fisher, M. Bohé, and J. L. Teyssié. Accumulation and toxicity of Cd, Zn, Ag, and Hg in four marine phytoplankters. *Marine Biology*, 18:201–213, 1984.

[18] N. S. Fisher and J. G. Fabris. Complexation of Cu, Zn and Cd by metabolites excreted from marine diatoms. *Marine Chemistry*, 11:245–255, 1982.

[19] T. Fuhrmann, S. Landwehr, M. El Rharbi-Kucki, and M. Sumper. Diatoms as living photonic crystals. *Applied Physics B*, 78:257–260, 2004.

[20] A. Gélabert, O. S. Pokrovsky, J. Viers, J. Schott, A. Boudou, A. Feurtet-Mazel, J. Mielczarski, E. Mielczarski, N. Mesmer-Dudons, and O. Spalla. Study of diatoms/aqueous interface. I. Acid-base equilibria and spectroscopic observation of freshwater and marine species. *Geochimica et Cosmochimica Acta*, 68:4039–4058, 2004.

[21] A. Gélabert, O. S. Pokrovsky, J. Viers, J. Scott, A. Boudou, and A. Feurtet-Mazel. Interaction between zinc and freshwater and marine diatom species: Surface complexation and Zn isotope fractionation. *Geochimica et Cosmochimica Acta*, 70:839–857, 2006.

[22] M. Gonzálves-Dávila. The Role of phytoplankton cells on the control of heavy metal concentration in seawater. *Marine Chemistry*, 48:215–236, 1995.

[23] M. Grätzel. Photoelectrochemical cells. *Nature*, 414:338–344, 2001.

[24] M. Grätzel. Dye-sensitized solar cells. *Journal of Photochemistry and Photobiology*, 4:145–153, 2003.

[25] R. R. R Guillard. *Culture of Marine Invertebrate Animals*. Plenum Press, 1957.

[26] T. W. Hamann, R. A. Jensen, B. F. Martinson, H. V. Ryswyk, and J. T. Hupp. Advancing beyond current generation dye-sensitized solar cells. *Energy and Environmental Science*, 1:66–78, 2008.

[27] C. E. Hamm, R. Merkel, O. Springer, P. Jurkojc, and C. Maier. Architecture and material properties of diatom shells provide effective mechanical protection. *Nature*, 421:841–843, 2003.

[28] P.J. Hansen. Effect of high ph on the growth and survival of marine phytoplankton: implications for species succession. *Aquatic microbial ecology*, 28:279–288, 2002.

[29] S. Hegde, D. D. Narale, and A. C. Anil. Sexual reproduction in *Odontella regia* (Schultze) Simonsen 1974 (Bacillariophyta). *Current Science*, 101, 2011.

[30] M. Hildebrand, L. G. Frigeri, and A. K. Davis. Synchronized growth of *Thalassiosira pseuodonana* (Bacillariophycaea) provides novel insights into cell-wall synthesis process in relation to the cell cycle. *Journal of Phycology*, 43:730–740, 2007.

[31] P. A. Hoskisson and G. Hobbs. Continuous culture- making a comeback? *Microbiology*, 151:3153–3159, 2005.

[32] T. Jaccard, D. Aritzegui, and K. J. Wilkinson. Incorporation of zinc into the frustule of the freshwater diatom *Stephanodiscus hantzschii*. *Chemical Geology*, 265:381–386, 2009.

[33] C. Jeffryes, T. Gutu, J. Jiao, and G. L. Rorrer. Metabolic Insertion of Nanostructured TiO2 into the patterned biosilica of the diatom pinnularia sp. by a two-stage bioreactor cultivation process. *American Chemical Society Nano*, 2:2103–2112, 2008.

[34] S. Klimmek and H. J. Stan. Comparative analysis of the biosorption of cadmium, lead, nickel, and zinc by algae. *Environmental Science and Technology*, 35:4283–4288, 2001.

[35] N. Kröger, R. Deutzmann, C. Bergsdorf, and M. Sumper. Species-specific polyamines from diatoms control silica morphology. *PNAS*, 97:14133–14138, 2000.

[36] N. Kröger and N. Poulson. Diatoms- From cell wall biogenesis to nanotechnology. *Annual Review of Genetics*, 42:83–107, 2008.

[37] W.M. Last and J.P. Smol. *Tracking environmental change using lake sediments: Terrestrial, algal, and siliceous indicators*, volume 3. Springer, 2001.

[38] T. Lebeau and M. J. Robert. Diatom cultivation and biotechnologically relevant products. Part II: Current and putative products. *Applied Microbiology and Biotechnology*, 60:624–632, 2003.

[39] J. C. Lewin. Silicon metabolism in diatoms. I. Evidence for the role of reduced sulfur compounds in silicon utilization. *The Journal of General Physiology*, 1954.

[40] R.A. Lincoln, K. Strupinski, and J.M. Walker. Biologically active compounds from diatoms. *Diatom research*, 5:337–349, 1990.

[41] S. Lippemeier, P. Hartig, and F. Colijn. Direct impact of silicate on the photosynthetic performance of the diatom *Thalassiosira weissflogii* asessed by on-and off-line PAM fluorescence measurements. *Journal of Plankton Research*, 21(2):269–283, 1999.

[42] AT Lombardi and PJ Wangersky. Particulate lipid class composition of three marine phytoplankters *Chaetoceros gracilis, Isochrysis galbana* (tahiti) and *Dunaliella tertiolecta* grown in batch culture. *Hydrobiologia*, 306:1–6, 1995.

[43] D. Losic, J. G. Mitchell, and N. H. Voelcker. Diatomaceous Lessons in Nanotechnology and Advanced Materials. *Advanced Materials*, 21:2947–2958, 2009.

[44] T. C. Malone, C. Garside, and P. J. Neale. Effects of silicate depletion on photosynthesis by diatoms in the plume of the Hudson River. *Marine Biology*, 58:197–204, 1980.

[45] V. Martin-Jézéquel, M. Hildebrand, and M. A. Brzekinski. Silicon metabolism in diatoms: Implication for growth. 36:821–840, 2000.

[46] KM McGinnis, TA Dempster, and MR Sommerfeld. Characterization of the growth and lipid content of the diatom *Chaetoceros muelleri*. *Journal of applied phycology*, 9:19–24, 1997.

[47] S. K. Mehta and J. P. Gaur. Use of algae for removing heavy metal ions from wastewater: progress and prospects. *Critical Reviews in Biotechnology*, 25:113–152, 2005.

[48] A. J. Miao, W. X. Wang, and P. Juneau. Comparison of Cd, Cu, and Zn toxic effects on four marine phytoplankton by pulse-amplitude-modulated fluorometry. *Environmental Toxicology and Chemistry*, 24:2603–2611, 2005.

[49] F. Monnet, N. Vaillant, P. Vernay, A. Coudret, and A. Hitmi. Relationship between PSII activity, CO2 fixation, and Zn, Mn and Mg contents of *Lolium perenne* under zinc stress. *Journal of Plant Physiology*, 158:1137–1144, 2001.

[50] C. M. Monteiro and P. M. L. Castro. Metal Uptake by Microalgae: Underlying Mechanisms and Practical Applications. *Biotechnology progress*, 00, 2012.

[51] F. M. M. Morel, J. R. Reinfelder, S. B. Roberts, C. P. Chamberlain, J. G. Lee, and D. Yee. Zinc and carbon co-limitation of marine phytoplankton. *Letters to nature*, 369:740–741, 1994.

[52] P. D. Nellist. *Scanning Transmission Electron Microscopy*, volume 1. Springer, 2007.

[53] D. W. O'Connel, C. Birkinshaw, and T. F. O'Dwyer. Heavy metal adsorbents prepared from the modfication of cellulose: A review. *Bioresource technology*, 99:6709–6724, 2008.

[54] E. Paasche. Silicon and the Ecology of Marine Plankton Diatoms. II. Silicate-uptake kinetics in five diatom species. *Marine Biology*, 19:262–269, 1973.

[55] E. Paasche. Silicon Content of Five Marine Plankton Diatom Species Measured with a Rapid Filter Method. *Limnology and Oceanography*, 25:474–480, 1980.

[56] J. Parkinson and R. Gordon. Beyond micromachining: the potential of diatoms. *Trends In Biotechnology*, 17, 1999.

[57] J. S. Parslow, P. J. Harrison, and P. A. Thompson. Saturated uptake kinetics: transient response of the marine diatom *Thalassiosira pseudonana* to ammonium, nitrate, silicate or phosphate starvation. *Marine Biology*, 83:51–59, 1984.

[58] O. S. Pokrovsky, G. S. Pokrovsky, A. Gélabert, J. Schott, and A. Boudou. Speciation of Zn associated with diatoms using X-ray absorption spectroscopy. *Environmental Science and Technology*, 39:4490–4498, 2005.

[59] N. Poulsen, C. Berne, J. Spain, and N. Kröger. Silica Immobilization of an enzyme through genetic engineering of the diatom *Thalassiosira pseudonana*. *Angewandte Chemie*, 46:1843–1846, 2007.

[60] N. M. Price and F. M. M. Morel. Cadmium and cobalt substitution for zinc in a marine diatom. *Nature*, 344:658–660, 1990.

[61] A. Rashid, E.L. Camm, and A. K. M. Ekramoddoullah. Molecular mechanism of action of Pb2+ and Zn2+ on water oxidizing complez of photosystem II. *FEBS letters*, 350:296–298, 1994.

[62] G-Y. Rhee. Continuous culture algal bioassays for organic pollutants in aquatic ecosystems. *Hydrobiologia*, 188/189:247–257, 1989.

[63] F. E. Round, R. M. Crawford, and D. G. Mann. *The diatoms: biology and morphology of the genera*. Cambridge University Press, 1990.

[64] A. Scheffel, Poulsen N., S. Shian, and N. Kröger. Nanopatterned protein microrings from a diatom that direct silica morphogenesis. *Proceedings of the National Academy of Sciences*, 108:3175–3180, 2011.

[65] A. Schröfel, G. Kratosová, M. Bohunická, E. Dobrocka, and I. Vávra. Biosynthesis of gold nanoparticles using diatoms- silica-gold and EPS-gold bionanocomposite formation. *Journal of Nanoparticle Research*, 13:3207–3216, 2011.

[66] J. Seckbach and J.P. Kociolek. *The Diatom World*, volume 19 of *Cellular Origin, Life in Extreme Habitats and Astrobiology*. Springer Netherlands, 2011.

[67] S. Sriharan, D. bagga, and TP Sriharan. Effects of nutrients and temperature on lipid and fatty acid production in the diatom *Hantzshia* di-60. *Applied biochemistry and biotechnology*, 24:309–316, 1990.

[68] L. D. Stefano, P. Maddalena, L. Moretti, I. Rea, I. Rendina, E. D. Tommasi, V. Mocella, and M. D. Stefano. Nano-biosilica from marine diatoms: A brand new material for photonic applications. *Superlattices and Microstructures*, 46:84–89, 2009.

[69] M. Sumper and Brunner E. Learning from diatoms: Nature's tools for the production of nanostructured silica. *Advanced Functional Materials*, 16:17–26, 2006.

[70] W. G. Sunda. Measurement of manganese, zinc and cadmium complexation in seawater using chelex ion exchange equilibria. *Marine Chemistry*, (365-378), 1984.

[71] W. G. Sunda and S. A. Huntsman. Feedback interactions between zinc and phytoplankton in seawater. *Limnology and Oceanography*, 37:25–40, 1992.

[72] W. G. Sunda and S. A. Huntsman. Cobalt and zinc interreplacement in marine phytoplankton: Biological and geochemical implications. *Limnology and Oceanography*, 40:1404–1417, 1995.

[73] W. G. Sunda and S. A. Huntsman. Processes regulating cellular metal accumulation and physiological effects: Phytoplankton as model systems. *The Science of The Total Environment*, 219:165–181, 1998.

[74] W.G. Sunda and S. A. Huntsman. Interactions Among Cu2+, Zn2+, and Mn2+ in Controlling Cellular Mn, Zn, and Growth Rate in the Coastal Alga *Chlamydomonas*. *Limnology and Oceanography*, 43:1055–1064, 1998.

[75] K. Thamatrakoln and M. Hildebrand. Silicon uptake in diatoms revisited: A model for saturable and nonsaturable uptake kinetics and the role of silicon transporters. *Plant Physiology*, 146:11397–1407, 2008.

[76] H. E. Townley, A. R. Parker, and H. White-Cooper. Exploitation of Diatom Frustules for Nanotechnology: Tethering Active Biomolecules. *Advanced Functional Materials*, 18:369–374, 2008.

[77] Ambrust E. V., J. A. Berges, Bowler C., and Green R. B. The Genome of the Diatom *Thalassiosira pseudonana*: Ecology, Evolution, and Metabolism. *Science*, 306, 2004.

[78] C. M. G. Van Den Berg. Determination of the zinc complexing capacity in seawater by cathodic stripping voltammetry of zinc-apdc complex ions. *Marine Chemistry*, 16:121–130, 1985.

[79] D. E. Varela, V. Willers, and D. W. Crawford. Effect of zinc availability on growth, morphology, and nutrient incorporation in a coastal and an oceanic diatom. *Journal of Phycology*, 47:302–312, 2011.

[80] H. Virgilio Perales-Vela and J. M. Peña-Castro. Heavy metal detoxification in eukaryotic microalgae. *Chemosphere*, 64:1–10, 2006.

[81] B. Volesky. Detoxification of metal-bearing effluents: biosorption for the next century. *Hydrometallurgy*, 59:203–216, 2001.

[82] J. C. Walsmsley, G. Jones, B. J. Lee, and R. K. Wild. High resolution imaging and analysis of grain boundaries in steel using a field emission auger microprobe. *Applied surface science*, 108:289–295, 1997.

[83] W. X. Wang, R. C. H. Dei, and Y. Xu. Responses of Zn Assimilation by Coastal Plankton to Macronutrients. *Limnology and Oceanography*, 46:1524–1534, 2001.

[84] S. M. Webb, G. G. Leppard, and J. F. Gaillard. Zinc speciation in a contaminated aquatic environment: Characterization of environmental particles by analytical electron microscopy. *Environmental Science and Technology*, 34:1926–1933, 2000.

[85] D Werner. *The Biology of Diatoms*, volume 13. University of Califorinia press, 1977.

[86] I. Worms, D. F. Simon, C. S. Hassler, and K. J. Wilkinson. Bioavailability of trace metals to aquatic microorganisms: importance of chemical, biological and physical processes on biouptake. *Biochemie*, 88:1721–1731, 2006.

[87] M. Wundram, D. Selmara, and M. Bahadirb. The chlamydomonas test: A new phytotoxicity test based on the inhibition of algal photosynthesis enables the assessment of hazardous leachates from waste disposals in salt mines. *Chemosphere*, 32:1623–1631, 1996.

[88] Y. Xu, D. Shi, Aristilde L., and F. M. M. Morel. The effect of pH on the uptake of zinc and cadmium in marine phytoplankton: possible role of weak complexes. *Limnology and Oceanography*, 57:293–304, 2012.

[89] H.-B. Xue, Stumm W., and L. Sigg. The binding of heavy metals to algal surfaces. *Water Research*, 22:917–926, 1988.

[90] S. Yamanaka, R. Yano, H. Usami, N. Hayashida, and M. Ohguchi. Optical Properties of diatom silica frustules with special reference to blue light. *Journal of Applied Physics*, 103, 2008.

[91] S. Yamasaki. Inductively Coupled Plasma Mass Spectrometry in Environmental Analysis. *Encyclopedia of Analytical Chemistry*, 2006.

[92] D. Yee and F. M. M. Morel. In vivo substitution of zinc by cobalt in carbonic anhydrase of a marine diatom. *Limnology and Oceanography*, 41:573–577, 1996.

[93] A. Zirino and S. Yamamoto. A pH dependent model for the chemical speciation of copper, zinc, cadmium, and lead in seawater. *Limnology and Oceanography*, 17:661–671, 1972.

A Experimental data

A.1 Experiment 1:

A.1.1 Filters

Table A.1: Concentration of Zn and Si in filters along with Relative Standard Deviation (RSD%) for Exp1.HD.

Sample	Zn			Si		
	ng mL^{-1}	RSD, %	Average, ng mL^{-1}	ng mL^{-1}	RSD, %	Average, ng mL^{-1}
Exp1.HD.Pre0-1	2.98	2.3	2.98	1659.31	2	1659.31
Exp1.HD.0.1	328.60	3.8	324.56	2244.82	2	2221.49
Exp1.HD.0.2	320.51	1.9		2198.15	4	
Exp1.HD.2.1	317.59	2.9	317.59	2640.87	2	2640.87
Exp1.HD.4.1	322.36	1.3	322.36	2988.84	3.5	2988.84
Exp1.HD.8.1	294.35	4.7	294.35	3207.98	1.5	3207.98
Exp1.HD.15.1	248.90	2	248.90	2194.48	1.1	2194.48
Exp1.HD.30.1	180.74	2.8	191.17	1933.62	4.4	1930.71
Exp1.HD.30.1 (2)	184.31	2.3		1927.79	2.3	
Exp1.HD.30.2	208.47	3.1		2849.38	4.1	
Exp1.HD.60.1	147.74	0.5	145.78	2296.31	1.9	2242.89
Exp1.HD.60.2	143.82	0.9		2189.48	4.3	
Exp1.HD.24h.1	56.15	5.8	56.58	4116.38	3	4375.96
Exp1.HD.24h.2	57.00	2.2		4635.53	1.6	
Exp1.HD.48h.1	50.87	3.4	50.99	3376.91	2.1	3339.48
Exp1.HD.48h.2	51.11	0.5		3302.05	3.1	

Table A.3: Amount (µg) of selected elements and relative standard deviation (RSD, %) in frustule analysis for Exp1.HD.

	Si		Zn		P		Fe		Ti		B	
	µg	RSD %	µg	RSD %	µg	RSD %	µg	RSD %	µg	RSD %	µg	RSD %
24 h	39.66	0.9	0.011	8.8	0.22	2.5	0.0014	5.1	0.0041	26.5	0.025	0.7
48 h	99.41	2.1	0.025	9.5	0.97	2.7	0.034	2.4	0.0088	38.4	0.054	0.5

A.1.2 Filtrates

Table A.2: Concentration of Zn and Si along with Relative Standard Deviation (RSD%) for Exp1.HD.

Sample	Zn			Si		
	µg L^{-1}	RSD, %	Average, µg L^{-1}	µg L^{-1}	RSD, %	Average, µg L^{-1}
Exp1.HD.Pre0-1	11.99	2.5	11.99	31.5	12.3	31.5
Exp1.HD.0.1	196.14	0.9	192.03	1610.74	11.3	1315.69
Exp1.HD.0.2	187.92	1.0		1020.65	1	
Exp1.HD.2.1	218.63	1.5	218.63	1464.83	24.7	1464.83
Exp1.HD.4.1	227.97	1.8	227.97	1483.20	2.1	1483.20
Exp1.HD.8.1	263.44	2	263.44	1329.90	10.8	1329.90
Exp1.HD.15.1	331.11	0.7	331.11	1483.37	3.7	1483.37
Exp1.HD.30.1	400.52	2.7	398.48	1406.35	8.5	1253.81
Exp1.HD.30.2	396.44	2		1101.27	3.2	
Exp1.HD.60.1	443.77	1.2	447.02	1086.47	4.3	1176.65
Exp1.HD.60.2	450.26	2.3		1266.83	5.3	
Exp1.HD.24h.1	538.58	2.2	546.58	-236.3*	7.2	8.43
Exp1.HD.24h.2	554.69	2.6		-90.20*	6.4	
Exp1.HD.48h.1	532.80	2.8	515.29	-226.27*	8.9	4.21
Exp1.HD.48h.2	497.78	1.5		-34.62*	6.3	

*Spectrophotometric values used

A.1.3 Frustules

A.2 Experiment 2:

A.2.1 Filters

Table A.4: Concentration of Zn and Si along with Relative Standard Deviation (RSD%) in filters for Exp2.LD.

Sample	Zn			Si		
	ng mL^{-1}	RSD, %	Average, ng mL^{-1}	ng mL^{-1}	RSD, %	Average, ng mL^{-1}
Exp2.LD.Pre0-1	3.39	2.3	3.39	2244.90	2.5	2244.90
Exp2.LD.0.1	77.44	1.6	76.67	2380.27	5.1	2424.51
Exp2.LD.0.2	75.90	4.9		2468.74	3.5	
Exp2.LD.2.1	76.11	0.8	76.11	2448.86	6.7	2448.86
Exp2.LD.4.1	77.30	1.2	77.30	2501.38	5.8	2501.38
Exp2.LD.8.1	74.99	1.6	74.99	2853.50	3.0	2853.50
Exp2.LD.15.1	69.75	2.9	69.75	2255.51	1.0	2255.51
Exp2.LD.30.1	59.25	1.4	59.63	2409.93	1.5	2416.93
Exp2.LD.30.2	60.01	0.6		2423.93	10.1	
Exp2.LD.60.1	45.42	2.2	47.75	2930.36	7.0	3068.88
Exp2.LD.60.2	50.08	0.2		3207.40	8.8	
Exp2.LD.24h.1	17.44	0.3	17.91	3998.24	5.4	4064.25
Exp2.LD.24h.2	18.39	0.7		4130.27	3.8	
Exp2.LD.48h.1	13.74	5.4	14.76	3159.38	7.5	3502.21
Exp2.LD.48h.2	15.79	1.6		3845.03	8.8	

Table A.6: Amount (µg) of selected elements and relative standard deviation (RSD, %) in frustule analysis for Exp2.LD.

	Si		Zn		P		Fe*		Ti		B	
	µg	RSD %	µg	RSD %	µg	RSD %	µg	RSD %	µg	RSD %	µg	RSD %
24 h	0.22	2.6	0.011	7.6	0.001	7.8	-	-	0.00014	71.2	-*	-*
48 h, 1	2.63	1	0.0038	9.9	0.03	8.6	-	-	0.0016	59.3	0.012	6.4
48 h, 2	2.83	0.3	0.0023	18.4	0.034	11	-	-	0.0010	20.2	0.011	8.3

*Negative values, not included in calculations

A.2.2 Filtrates

Table A.5: Concentrations of Zn and Si along with Relative Standard Deviation (RSD%) in filtrates for Exp2.LD.

Sample	Zn			Si		
	µg L^{-1}	RSD, %	Average, µg L^{-1}	µg L^{-1}	RSD, %	Average, µg L^{-1}
Exp2.LD.Pre0-1	11.81	3.5	11.81	15.6	12.3	31.5
Exp2.LD.0.1	45.56	1.8	39.19	1491.4	11.3	1315.69
Exp2.LD.0.2	32.81	0.4		924.63	1	
Exp2.LD.2.1	47.22	1.6	47.22	1620.25	24.7	1464.83
Exp2.LD.4.1	50.62	2.6	50.62	1693.56	2.1	1483.20
Exp2.LD.8.1	54.54	1.2	54.54	1524.88	10.8	1329.90
Exp2.LD.15.1	59.54	2.5	59.54	1523.80	3.7	1483.37
Exp2.LD.30.1	71.50	2.4	68.83	1387.25	18.9	1371.21
Exp2.LD.30.2	66.15	0.2		1355.18	3.9	
Exp2.LD.60.1	87.63	0.5	84.45	945.78	8.9	967.96
Exp2.LD.60.2	81.26	2.1		990.15	7.8	
Exp2.LD.24h.1	119.89	1.5	119.97	187.00	12.7	187.00
Exp2.LD.24h.2	120.06	1.2		-101.26*	8.2	
Exp2.LD.48h.1	123.11	2.9	124.46	33.16	12.7	160.71
Exp2.LD.48h.2	125.81	1.6		288.26*	5.9	

*Not included in average

A.2.3 Frustules

A.3 Sum of Zn fraction from filters and filtrates

Table A.7: Sum of the Zn fractions detected in filter and filtrates of Exp1.HD and Exp2.LD. The metal fraction from the 'Pre-zero' sample is not included.

Timepoint	Exp1.HD	Exp2.LD
	Sum [Zn], μmol L^{-1}	Sum [Zn], μmol L^{-1}
0	7.89	1.77
2	8.19	1.89
4	8.41	1.96
8	8.52	1.98
15	8.86	1.98
30	9.09	1.96
60	9.05	2.02
24	9.21	2.11
48	8.65	2.13
Average	8.65	1.98

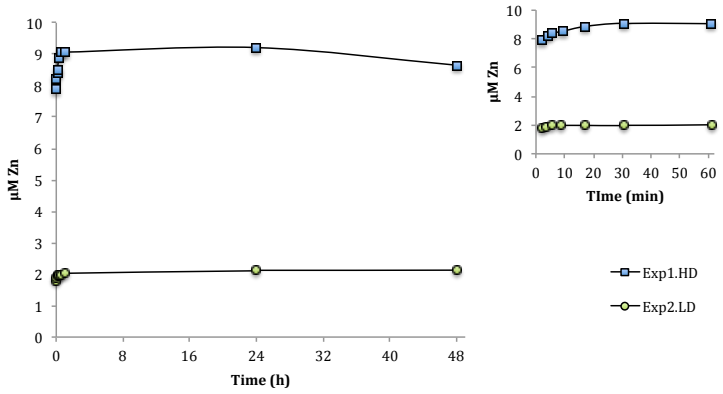

Figure A.1: Sum of Zn fractions detected in filters and filtrates for Exp1.HD and Exp2.LD.

A.4 Control experiment and frustules, and blanks

A.4.1 Control experiment and blanks

Table A.8: Filtrate concentration of Zn and Si in the control experiment. Average values are reported.

Sample	Zn		Si	
	μg.L^{-1}	RSD, %	μg.L^{-1}	RSD, %
CM.0	487.9	3.6	3270.2	3.6
CM.30	470.8	4.1	3104.1	5.1
CM.60	469.9	4.6	3406.2	4.6
CM.24h	544.7	2.4	2151.3	2.4
CM.48h	559.9	2.9	3247.5	2.9

Table A.9: Blanks used in the correction of filtrate and filter values. B.MQ- blank with Milli-Q water, STB- sample treated blank (soaked filters in sample).

Correction sample	Type of correction	Zn, $\frac{\text{Blank (ng mL\^-1)}}{\text{Sample (ng mL\^-1)}}$	Si, $\frac{\text{Blank (ng mL\^-1)}}{\text{Sample (ng mL\^-1)}}$	Zn µg mL^{-1}	Si µg mL^{-1}
B.MQ	Filtrate corrections: Equipment	-	-	0.69	0
STB.Pre0.2	Filter corrections: fraction of medium left on filter	0.07	0.01		
STB.0.1		0.02	0.004		
STB.2.1		0.01	0.008		
STB.4.1		0.11	0.006		
STB.8.1		0.01	0.004		
STB.15.1		0.02	0.008		
STB.30.1		0.06	0.013		
STB.60.1		0.05	0.019		
STB.24h.1		0.17	-		
STB.48h.1		0.23	0.005		

A.4.2 Control frustules

Table A.10: Amount (µg) of selected elements and relative standard deviation (RSD, %) in the analysis of the control frustules.

Cleaning method	Parallell	Si		Zn		P		Fe		Ti		B	
		µg	RSD %	µg	RSD %	µg	RSD %	µg	RSD %	µg	RSD %	µg	RSD %
SDS/EDTA	1	206.67	0.5	-*	-*	2.85	7.8	-*	-*	0.23	3.5	0.28	3.5
	2	204.54	1.4	-*	-*	2.94	8.6	-*	-*	0.26	13.6	0.27	3.4
H_2O_2	1	212.61	1.8	0.05	9.5	0.18	1.7	0.27	2	0.02	18.2	0.05	8.4
	2	206.02	1.7	0.04	0.8	0.18	5.7	0.26	1	0.06	110.5	0.04	5.1

*Negative values